5. Merker HJ, Günther T (1997) Testis damage induced by zinc deficiency in rat. *J Trace Element* 11:19–22.
6. Boran C, Ozkan KU (2004) The effect of zinc therapy on damaged testis in prepubertal rats. *Pediatr Surg Int* 20:444–448.
7. Henkel R, et al. (2005) Molecular aspects of declining sperm motility in older man. *Fert Ster* 84:1430–1437.
8. Morisawa M, Yoshida M (2005) Activation of motility and chemotaxis in the spermatozoa: From invertebrates to humans. *Reprod Med Biol* 4:101–114.
9. Clapper DL, Davis JM, Lamothe PJ, Patton C, Epel D (1985) Involvement of zinc in the regulation of pHi, motility, and acrosome reactions in sea urchin sperm. *J Cell Biol* 100:1817–1824.
10. Stoltenberg M, et al. (1997) Autometallographic demonstration of zinc ion in rat sperm cell. *Mol Hum Reprod* 3:763–767.
11. Morisawa M, Mohri H (1972) Heavy metals and spermatozoan motility. I. distribution of iron, zinc and copper in sea urchin spermatozoa. *Exp Cell Res* 70:311–316.
12. Miura T, Yamauchi K, Nagahama Y, Takahashi H (1991) Induction of spermatogenesis in male Japanese eel, *Anguilla japonica*, by a single injection of human chorionic gonadotropin *Zool Sci* 8:63–73.
13. Miura T, Yamauchi K, Takahashi H, Nagahama Y (1991) Hormonal induction of all stages of spermatogenesis *in vitro* in the male Japanese eel (*Anguilla japonica*). *Proc Natl Acad Sci USA* 88:5774–5778.
14. Miura T, Yamauchi K, Takahashi H, Nagahama Y (1991) Human chorionic gonadotropin induced all stages of spermatogenesis *in vitro* in the male Japanese eel (*Anuilla japonica*). *Dev Biol* 146:258–262.
15. Miura T, Miura C (2001) Japanese eel: A model for analysis of spermatogenesis. *Zool Sci* 18:1055–1063.
16. Miura T, Higuchi M, Ozaki Y, Ohta T, Miura C (2006) Progestin is an essential factor for the initiation of the meiosis in spermatogenic cell of the eel. *Proc Natl Acad Sci USA* 103:7333–7338.
17. Yamaguchi S, et al. (2007) Effects of lead, molybdenum, rubidium, arsenic, and organochlorines on spermatogenesis in fish: Monitoring at Mekong Delta area and *in vitro* experiment. *Aquat Toxicol* 83:43–51.
18. Miura T, et al. (1999) Estradiol-17β stimulated the renewal of spermatogonial stem cell in males. *Biochem Biophysical Res Comm* 264:230–234.
19. Hidiroglou M, Knipfel JE (1984) Zinc in mammalian sperm: A review. *J Dairy Sci* 67:1147–1156.
20. Sørensen MB, et al. (1998) Histochemical tracing of zinc ions in the rat testis. *Mol Hum Reprod* 4:423–428.
21. Elgazar V, et al. (2005) Zinc-regulating proteins, ZnT-1, and Metallothionein I/II are present in different cell populations in the mouse testis. *J Histochem Cytochem* 53:905–912.
22. Sugihara T, Wadhwa R, Kaul SC, Mitsui YA (1999) novel testis-specific metallothionein-like protein, tesmin, is an early marker of male germ cell differentiation. *Genomics* 57:130–136.
23. Olesen C, Møller M, Byskov AG (2004) Tesmin transcription is regulated differently during male and female meiosis. *Mol Reprod Dev* 67:116–126.
24. Chi ZH, et al. (2009) ZNT7 and Zn^{2+} are present in different cell populations in the mouse testis. *Histol Histopathol* 24:25–30.
25. Guan Z, et al. (2003) Kinetic indentification of a mitochondrial zinc uptake transport process in prostate cells. *J Inorg Biochem* 97:199–206.
26. Costello LC, Guan Z, Franklin RB, Feng P (2004) Metallothionein can function as a chaperone for zinc uptake transport into prostate and liver mitochondria. *J Inorg Biochem* 98:664–666.
27. Zelewski PD, Forbes IJ, Betts WH (1993) Correlation of apoptosis with change in intracellular labile Zn(II) using Zinquin [(2-methyl-8-*p*-toluenesulphonamido-6- quinolyloxy)acetic acid], a new specific fluoprescent probe for Zn(II), *Biochem J* 296:403–408.
28. Nakatani T, Tawaramoto M, Kennedy DO, Kojima A, Matsui-Yuasa I (2000) Apoptosis induced by chelation of intracellular zinc is associated with depletion of cellular reduced glutathione levels in rat hepatocytes. *Chem-Biol Interact* 125:151–163.
29. Ho LH, et al. (2004) Labile zinc and zinc transporter ZnT4 in mast cell granules: Role in regulation of caspase activation and NF-κB translocation. *J Immunol* 172:7750–7760.
30. Jankowski-Henning MA, Clegg MS, Daston GP, Rogers JM, Keen CL (2000) Zinc-deficient rat embryos have increased caspase 3-like activity and apoptosis. *Biochem Biophysic Res Commun* 271:250–256.
31. Fukamachi Y, et al. (1998) Zinc suppresses apoptosis of U937 cells induced by hydrogen peroxide through an increase of the bcl-2/bax ratio. *Biochem Biophys Res Commun* 246:364–369.
32. Truong-Tran AQ, Carter J, Ruffin RE, Zalewski PD (2001) The role of zinc in caspase activation and apoptotic cell death. *Biometals* 14:315–330.
33. Chesters JK, Boyne R (1991) Nature of the Zn^{2+} requirement for DNA synthesis by 3T3 cells. *Experiment Cell Res* 192:631–634.
34. Freedman LP (1992) Anatomy of the steroid receptor zinc finger region. *Endocrine Rev* 13:129–145.
35. Rossi P, et al. (2004). Analysis of the gene expression profile of mouse male meiotic germ cells. *Gene Expr Patterns* 4:267–281.267–281.
36. Sørensen MB, Stoltenberg M, Danscher G, Ernst E (1999) Chelation of intracellular zinc ions affects human sperm cell motility. *Mol Human Reprod* 5:338–341.
37. Turner RM (2006) Moving to the beat: A review of mammalian sperm motility regulation. *Reprod Fert Devlop* 18:25–38.
38. Supuran CT, Scozzafava A, Casini A (2003) Carbonic anhydrase inhibitors. *Med Res Rev* 23:146–189.
39. Rana U, et al. (2008) Zinc binding ligands and cellular zinc trafficking: Apo- metallothionein, glutathione, TPEN, proteomic zinc, and Zn-sp1. *J Inorg Biochem* 102:489–499.
40. Miura T, Ando A, Miura C, Yamauchi K (2002) Comparative studies between *in vivo* and *in vitro* spermatogenesis of Japanese eel (*Anguilla japonica*). *Zool Sci* 19:321–329.
41. Hirano T, Kikuchi K, Urano Y, Nagano T (2002) Improvement and biological applications of fluorescent probes for zinc, ZnAFs. *J Am Chem Soc* 124:6555–6562.
42. Miura C, Takahashi N, Michino F, Miura T (2005) The effects of *para*-nonylphenol on Japanese eel (*Anguilla japonica*) spermatogenesis. *In Vitro Aquat Toxicol* 71:133–141.
43. Ohta H, Izawa T (1996) Diluent for cool storage of the Japanese eel (*Anguilla japonica*) spermatozoa. *Aquaculture* 142:107–118.

ORGANIC LETTERS

2009
Vol. 11, No. 13
2732–2735

Anion Sensor-Based Ratiometric Peptide Probe for Protein Kinase Activity

Kazuya Kikuchi,[†,‡,§] Shigeki Hashimoto,[†,⊥] Shin Mizukami,[‡,§] and Tetsuo Nagano*[,‡]

Graduate School of Pharmaceutical Sciences, The University of Tokyo, 7-3-1 Hongo, Bunkyo-ku, Tokyo 113-0033, Japan and PRESTO, JST Corporation, Kawaguchi, Saitama, Japan

tlong@mol.f.u-tokyo.ac.jp

Received April 7, 2009

ABSTRACT

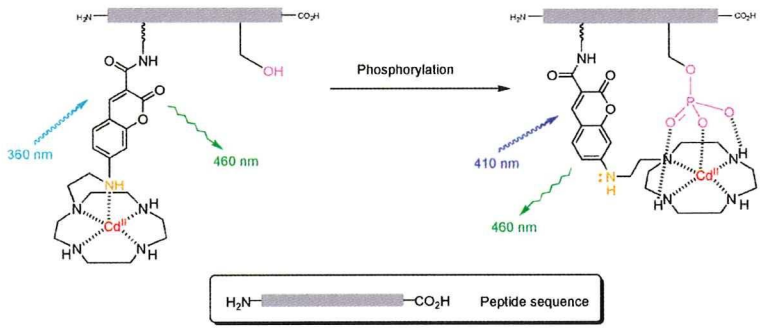

A new fluorescent sensor consisting of Cd^{II}-cyclen appended aminocoumarin and a substrate peptide for protein kinase A (PKA) has been designed. Upon phosphorylation by PKA, the metal complex moiety binds to a phosphorylated residue, which in turn displaces the coumarin fluorophore, and this event results in ratiometric change of excitation spectrum in neutral aqueous solution.

Signal transduction pathways provide mechanisms for transducing external signals to intracellular biological responses. Protein kinases modulate the activity of their target proteins by phosphorylating serine, threonine and tyrosine residues within the intact proteins in these pathways. A great number of kinases have been discovered, and the characterization of their roles in complicated signaling pathways is now a very active research area.[1] The development of an analytical tool that can enable monitoring of the temporal and spatial dynamics of cellular kinases would therefore contribute substantially to a better understanding of signal transduction mechanisms.[2]

Various approaches to monitor the activities of protein kinases have been made,[3,4] one of which is the use of fluorophore-labeled peptide substrates.[5] Traditional peptide probes contain a polarity-sensitive fluorophore near the site

[†] JST corporation.

[‡] The University of Tokyo.

[⊥] Present address: Faculty of Industrial Science and Technology, Tokyo University of Science, Oshamanbe, Hokkaido 049-3514, Japan.

[§] Present address: Graduate School of Engineering, Osaka University, 2-1 Yamada-oka, Suita City, Osaka 565-0871, Japan.

(1) *Chem. Rev.* **2001**, *101*, issue 8: Protein Phosphorylation and Signaling.

(2) (a) Eisele, F.; Owen, D. J.; Waldmann, H. *Bioorg. Med. Chem.* **1999**, *7*, 193–224. (b) Lawrence, D. S. *Acc. Chem. Res.* **2003**, *36*, 401–409.

(3) (a) Nagai, Y.; Miyazaki, M.; Aoki, R.; Zama, T.; Inouye, S.; Hirose, K.; Iino, M.; Hagiwara, M. *Nat. Biotechnol.* **2000**, *18*, 313–316. (b) Hofmann, R. M.; Cotton, G. J.; Chang, E. J.; Vidal, E.; Veach, D.; Bornmann, W.; Muir, T. W. *Bioorg. Med. Chem. Lett.* **2001**, *11*, 3091–3094. (c) Kurokawa, K.; Mochizuki, N.; Ohba, Y.; Mizuno, H.; Miyawaki, A.; Matsuda, M. *J. Biol. Chem.* **2001**, *276*, 31305–31310. (d) Ting, A. Y.; Kain, K. H.; Klemke, R. L.; Tsien, R. Y. *Proc. Natl. Acad. Sci. U.S.A.* **2001**, *98*, 15003–15008. (e) Sato, M.; Ozawa, T.; Inukai, K.; Asano, T.; Umezawa, Y. *Nat. Biotechnol.* **2002**, *20*, 287–294.

(4) (a) Ohuchi, Y.; Katayama, Y.; Maeda, M. *Analyst* **2000**, *125*, 1905–1907. (b) Ojida, A.; Inoue, M.; Mito-oka, Y.; Hamachi, I. *J. Am. Chem. Soc.* **2003**, *125*, 10184–10185. (c) Ojida, A.; Mito-oka, Y.; Sada, K.; Hamachi, I. *J. Am. Chem. Soc.* **2004**, *126*, 2454–2463.

(5) (a) McIlroy, B. K.; Walters, J. D.; Johnson, J. D. *Anal. Biochem.* **1991**, *195*, 148–152. (b) Post, P. L.; Trybus, K. M.; Taylor, D. L. *J. Biol. Chem.* **1994**, *269*, 12880–12887. (c) Higashi, H.; Sato, K.; Omori, A.; Sekiguchi, M.; Ohtake, A.; Kudo, Y. *NeuroReport* **1996**, *7*, 2695–2700. (d) Higashi, H.; Sato, K.; Ohtake, A.; Omori, A.; Yoshida, S.; Kudo, Y. *FEBS Lett.* **1997**, *414*, 55–60. (e) Yeh, R.-H.; Yan, X.; Cammer, M.; Bresnick, A. R.; Lawrence, D. S. *J. Biol. Chem.* **2002**, *277*, 11527–111532.

10.1021/ol9006508 CCC: $40.75
Published on Web 06/04/2009

of phosphorylation, and this serves to signal the change of environment upon phosphorylation. The groups of Lawrence and Imperiali have developed chelator-appended fluorescent peptides for monitoring kinase activities.[6] Upon phosphorylation, these peptides show a significant fluorescence intensity increase owing to the formation of divalent alkaline earth metal complexes coordinated to the newly generated phosphate group and the fluorophore.

Fluorescence measurement at a single wavelength without much shift of either the excitation or emission wavelength can be influenced by artifacts associated with the microscopic imaging system. To reduce the influence of such factors, ratiometric measurement is utilized, namely, simultaneous recording of the fluorescence intensities at two wavelengths and calculation of their ratio.[7] For this approach, probes that signal phosphorylation via a shift of either excitation or emission wavelength are required.

We have designed a fluorescent anion sensor, consisting of 7-aminotrifluoromethylcoumarin as a fluorescent reporter and Cd^{II}-cyclen (1,4,7,10-tetraazacyclododecane) as an anion host.[8] This sensor molecule can detect phosphate anion species, such as pyrophosphate, with high sensitivity in aqueous neutral solution. As an extension of the anion sensor concept, we have newly designed an anion sensor-appended peptide substrate for protein kinases. Here we describe the sensing of a kinase-mediated phosphorylation event by a fluorescent peptide sensor. This novel class of peptide probe exhibited a shift of excitation spectrum upon phosphorylation, enabling ratiometric measurement of kinase activity. This technique can provide more precise data than measurement at a single wavelength, canceling out the influence of variations in instrument efficiency, content of effective dye, and so forth.

The operational concept of the peptide sensor is schematically presented in Scheme 1. This peptide sensor consists of

Scheme 1. Schematic Representation of our Peptide Sensor for Phosphorylation

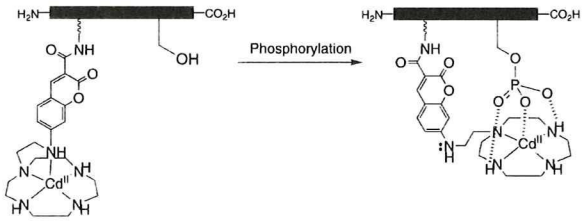

an anion sensor and a phosphorylation target peptide sequence. The sensing moiety is positioned near the target hydroxyl amino acid residue. In neutral aqueous solution, Cd^{II} of the cyclen complex is coordinated by the four nitrogen atoms of cyclen and the aromatic 7-amino group of coumarin.[9] When a negatively charged phosphate group coordinates to Cd^{II} as the fifth ligand, the aromatic 7-amino group is displaced from the metal. The anion sensor signals this replacement, because the increase of electron density of the 7-amino group induces a red shift of the excitation spectrum. We have designed peptide sensor **1** for protein kinase A (PKA) as shown in Scheme 2. The sequence of the peptide

Scheme 2. Sequence of Peptide Sensor and its Phosphorylated Standard Employed in This Study

Sensor-$(CH_2)_5$-LRRASLG-$CONH_2$ **1**

Sensor-$(CH_2)_5$-LRRApSLG-$CONH_2$ **1P**

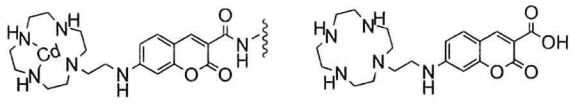

Sensor **2**

sensor is known as Kemptide and has been shown to be a good substrate for the kinase.[10] The sensing moiety is positioned at the N-terminus of the peptide through an alkyl tether, enabling recognition of a phosphorylated serine residue. We also designed a phosphorylated sensor **1P** to estimate preliminarily the extent of spectral change upon phosphorylation.

The cyclen-appended 7-aminocoumarincarboxylic acid **2** was synthesized according to the established procedure.[8] The peptide sequence was synthesized using Fmoc solid-phase chemistry on an automated peptide synthesizer and the ligand **2** was manually coupled to the amino linker. The resulting peptide conjugate was metalated with $Cd(ClO_4)_2$ to give the desired peptide sensor **1**. Phosphorylated peptide sensor **1P** was prepared by protein kinase-mediated phosphorylation of the peptide conjugate followed by metalation with Cd^{II}. The structures of **1** and **1P** were confirmed by MALDI-TOF MS (matrix assisted laser desorption/ionization-time-of-flight mass spectrometry) and quantitative amino acid analysis.

We tested the sensing ability of peptide sensor **1** by comparing the excitation spectrum with that of the phosphorylated product, **1P** (see Supporting Information). Upon phosphorylation, the excitation intensity at 360 nm decreased, whereas the intensity at 410 nm increased. The ratio of the excitation intensities (410 nm/360 nm) changed

(6) (a) Chen, C. A.; Yeh, R. H.; Lawrence, D. S. *J. Am. Chem. Soc.* **2002**, *124*, 3840–3841. (b) Shults, M. D.; Imperiali, B. *J. Am. Chem. Soc.* **2003**, *125*, 14248–14249.

(7) (a) Tsien, R. Y.; Harootunian, A. T. *Cell Calcium* **1990**, *11*, 93. (b) Kikuchi, K.; Takakusa, H.; Nagano, T. *Trends in Anal. Chem.* **2004**, *23*, 407–415.

(8) Mizukami, S.; Nagano, T.; Urano, Y.; Odani, A.; Kikuchi, K. *J. Am. Chem. Soc.* **2002**, *124*, 3920–3925.

(9) (a) Koike, T.; Watanabe, T.; Aoki, S.; Kimura, E.; Shiro, M. *J. Am. Chem. Soc.* **1996**, *118*, 12696–12703. (b) Aoki, S.; Kaido, S.; Fujioka, H.; Kimura, E. *Inorg. Chem.* **2003**, *42*, 1023–1030.

(10) (a) Kemp, B. E.; Graves, D. J.; Benjamini, E.; Krebs, E. G. *J. Biol. Chem.* **1977**, *252*, 4888–4894. (b) Kemp, B. E. *J. Biol. Chem.* **1980**, *255*, 2914–2918.

1.8-fold (from a value of 0.54 to 0.96), demonstrating that peptide phosphorylation can be detected with an anion sensor.[11]

To investigate the utility of the compound as a fluorescent probe for protein kinases, we measured the time-dependent change of the excitation spectrum of **1** treated with ATP (adenosine 5′-triphosphate) and PKA catalytic subunit (Figure 1). The phosphorylation reaction

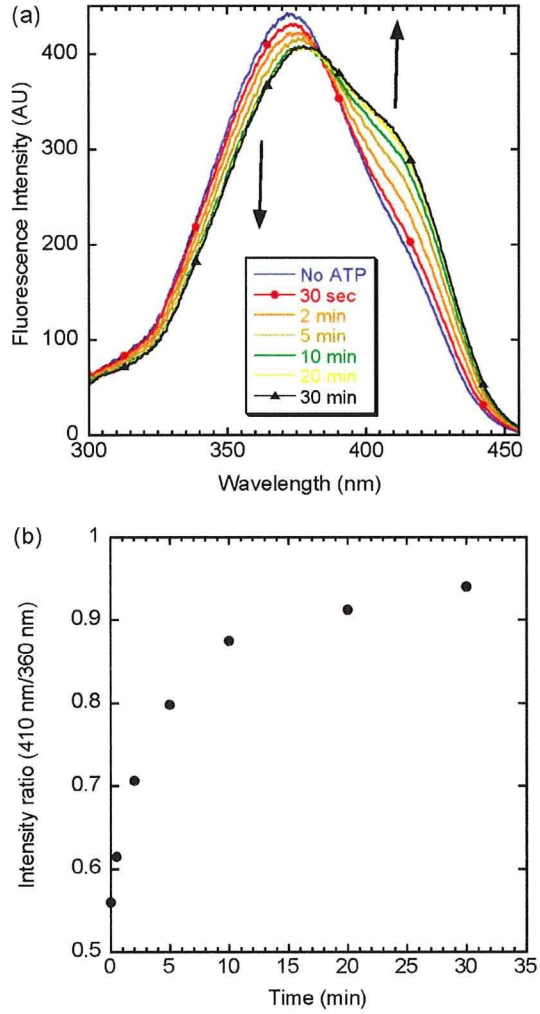

Figure 1. (a) Time course of the excitation spectra of **1** treated with PKA catalytic subunit. The peptide sensor **1** (1.3 μM) was incubated in 50 mM HEPES (pH 7.4), 5 mM $Mg(OAc)_2$ containing 4.3 nM catalytic subunit and 3.3 μM ATP at 23 ± 0.1 °C. (b) Plot of intensity ratio (410 nm/360 nm) versus reaction time.

was initiated by the addition of ATP to a mixture of **1** and the catalytic subunit. Though ATP strongly coordinates to the Cd^{II} complex of the anion sensor, addition of this organic polyanion had no significant effect on the excitation spectrum under the conditions employed.[12] As can be seen from Figure 1, the excitation spectra of **1** changed ratiometrically; the intensity at 360 nm decreased with a concomitant intensity increase at 410 nm. The ratio of excitation intensity (410 nm/360 nm) increased 1.7 fold after 30 min reaction time, and this is similar to the value obtained by comparison of the excitation spectra of authentic **1** and **1P**. The phosphorylation reaction was accelerated by increasing the quantity of kinase employed for the reaction (see Supporting Information).

We further carried out an inhibition experiment using the heat-stable inhibitor protein of PKA (PKI), which acts competitively with respect to the phosphoryl-accepting substrate (Figure 2).[13] Dose-dependent inhibition of kinase

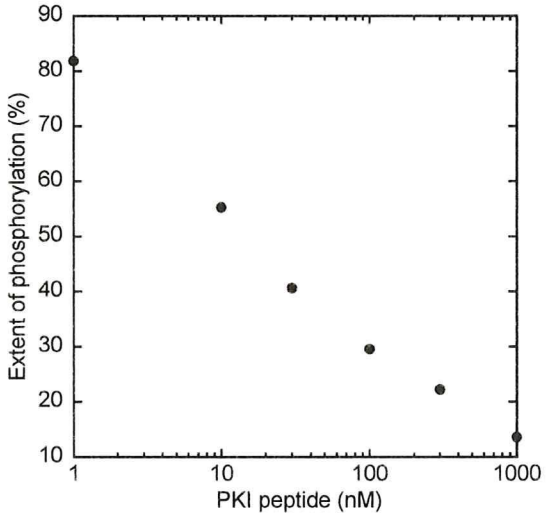

Figure 2. Titration of PKA-mediated phosphorylation of **1** with PKI peptide. The phosphorylation reaction was carried out in 50 mM HEPES (pH 7.4), 5 mM $Mg(OAc)_2$ containing 1.0 μM **1**, 4.3 nM catalytic subunit, 3.3 μM ATP and various amounts of PKI peptide at 23 ± 0.1 °C. Extent of phosphorylation (%) was determined by comparing the intensity ratio increase at the early phase of the reaction (0−5 min) with that of the control.

activity by PKI peptide was observed for phosphorylation of **1** with an IC_{50} (half maximal inhibitory concentration) of ca. 15 nM under the conditions employed. This result indicates that the ratiometric spectral change is caused by PKA-mediated phosphorylation of **1**.[14]

In conclusion, we have developed a new fluorescent probe for protein kinase based on the anion sensing principle. It has been demonstrated that this peptide probe can be used

(11) A significant shift of the absorption peak was also observed for the Cd^{II} complex of methylated compound **2** upon addition of pyrophosphate anion. Titration of the complex with pyrophosphate gave the Kd value of 53 μM.

(12) The addition of more than three equivalents of ATP to the peptide sensor **1** induced an excitation change at two wavelengtth (360 and 410 nm), which indicates the coordination of ATP to the metal complex moiety.

(13) (a) Cheng, H. C.; Kemp, B. E.; Pearson, R. B.; Smith, A. J.; Misconi, L.; Van Patten, S. M.; Walsh, D. A. *J. Biol. Chem.* **1986**, *261*, 989–992. (b) Glass, D. B.; Cheng, H. C.; Mueller, L. M.; Reed, J.; Walsh, D. A. *J. Biol. Chem.* **1989**, *264*, 8802–8810.

to continuously monitor kinase-mediated phosphorylation through intensity measurements at two wavelengths. This peptide sensor might serve as the basis for a range of anion sensor-based phosphorylation probes for many different protein kinases.

(14) Actual phosphorylation of peptide sensor **1** was confirmed by analyzing the reaction mixture, using C_{18} reverse-phase HPLC (high-performance liquid chromatography). Time-dependent production of phosphorylated product was observed when the sensor **1** was exposed to PKA catalytic subunit. The phosphorylated product co-eluted with authentic standard **1P** from the HPLC column.

Acknowledgment. We thank Prof. H. Mihara and Dr. T. Takahashi at the Tokyo Institute of Technology for technical assistance in peptide synthesis.

Supporting Information Available: Synthesis of anion sensor and peptide conjugate, fluorescence experiment, protein kinase assay. This material is available free of charge via the Internet at http://pubs.acs.org.

OL9006508

7630 *Inorg. Chem.* **2009**, *48*, 7630–7638
DOI: 10.1021/ic900247r

Inorganic Chemistry
Article

Design and Synthesis of Coumarin-Based Zn^{2+} Probes for Ratiometric Fluorescence Imaging

Shin Mizukami, Satoshi Okada, Satoshi Kimura, and Kazuya Kikuchi*

Division of Advanced Science and Biotechnology, Graduate School of Engineering, Osaka University, 2-1 Yamadaoka, Suita, Osaka 565-0871, Japan

Received February 5, 2009

The physiological roles of free Zn^{2+} have attracted great attention. To clarify those roles, there has been a need for ratiometric fluorescent Zn^{2+} probes for practical use. We report the rational design and synthesis of a series of ratiometric fluorescent Zn^{2+} probes. The structures of the probes are based on the 7-hydroxycoumarin structure. We focused on the relationship between the electron-donating ability of the 7-hydroxy group and the excitation spectra of 7-hydroxycoumarins, and exploited that relationship in the design of the ratiometric probes; as a result, most of the synthesized probes showed ratiometric Zn^{2+}-sensing properties. Then, we designed and synthesized ratiometric Zn^{2+} probes that can be excited with visible light, by choosing adequate substituents on coumarin dyes. Since one of the probes could permeate living cell membranes, we introduced the probe to living RAW264 cells and observed the intracellular Zn^{2+} concentration via ratiometric fluorescence microscopy. As a result, the ratio value of the probe changed quickly in response to intracellular Zn^{2+} concentration.

Introduction

Zinc is one of the most heavily studied metals in biology. The biological roles of Zn^{2+} have been studied since the 1940s; the main studies focused on its biochemical roles, either as structural elements in enzymes and transcription factors or as the catalytic elements in enzymatic activity centers.[1] These Zn^{2+}s are thought to be bound strongly to peptides or proteins. Meanwhile, the physiological roles of free Zn^{2+} have recently attracted great attention, mainly in neurology.[2] Generally, to study the physiological roles of biomolecules in living cells or tissues, it is quite useful to visualize them under microscopes; fluorescent probes are useful in this endeavor. For example, rapid progress in physiological Ca^{2+} studies has been accomplished through the use of fluorescent Ca^{2+} probes such as fura-2, fluo-3, and succeeding compounds.[3] The success of Ca^{2+} probes has, in turn, encouraged the development of fluorescent probes for other various biomolecules.

With regards to fluorescent probes for Zn^{2+},[4] the pioneering compound was TSQ (*N*-(6-methoxy-8-quinolyl)-*p*-toluenesulfonamide), as reported by Frederickson et al.[5] Although it was difficult for TSQ to be applied to live cell imaging for hydrophobicity, its hydrophilic derivative, Zinquin, enabled the fluorescence microscopic imaging of free Zn^{2+}.[6] Such quinoline-based probes are, however, excited by ultraviolet light, thus inducing cell damage and autofluorescence from fluorescent biomolecules such as flavin derivatives. Thus, the fluorescent probes for longer-wavelength excitation have been actively developed by several groups.[7–10] Since most of these probes are fluorescein-based, they are much brighter than

*To whom correspondence should be addressed. E-mail: kkikuchi@mls.eng.osaka-u.ac.jp.

(1) (a) Prasad, A. S. *Biochemistry of Zinc*; Plenum Press: New York, 1993. (b) Vallee, B. L.; Falchuk, K. H. *Physiol. Rev.* **1993**, *73*, 79–118.

(2) Frederickson, C. J.; Koh, J. -Y.; Bush, A. I. *Nat. Rev. Neurosci.* **2005**, *6*, 449–462.

(3) Kao, J. P. Y. *Methods Cell Biol.* **1994**, *40*, 155–181.

(4) See following reviews: (a) Burdette, S. C.; Lippard, S. J. *Coord. Chem. Rev.* **2001**, *216–217*, 333–361. (b) Kimura, E.; Aoki, S. *Biometals* **2001**, *14*, 191–204. (c) Kikuchi, K.; Komatsu, K.; Nagano, T. *Curr. Opin. Chem. Biol.* **2004**, *8*, 182–191. (d) Dai, Z.; Canary, J. W. *New J. Chem.* **2007**, *31*, 1708–1718.

(5) Frederickson, C. J.; Kasarskis, E. J.; Ringo, D.; Frederickson, R. E. *J. Neurosci. Methods* **1987**, *20*, 91–103.

(6) Zalewski, P. D.; Forbes, I. J.; Betts, W. H. *Biochem. J.* **1993**, *296*, 403–408.

(7) (a) Hirano, T.; Kikuchi, K.; Urano, Y.; Higuchi, T.; Nagano, T. *Angew. Chem., Int. Ed.* **2000**, *39*, 1052–1054. (b) Hirano, T.; Kikuchi, K.; Urano, Y.; Higuchi, T.; Nagano, T. *J. Am. Chem. Soc.* **2000**, *122*, 12399–12400. (c) Hirano, T.; Kikuchi, K.; Urano, Y.; Nagano, T. *J. Am. Chem. Soc.* **2002**, *124*, 6555–6562. (d) Komatsu, K.; Kikuchi, K.; Kojima, H.; Urano, Y.; Nagano, T. *J. Am. Chem. Soc.* **2005**, *127*, 10197–10204.

(8) (a) Walkup, G. K.; Burdette, S. C.; Lippard, S. J.; Tsien, R. Y. *J. Am. Chem. Soc.* **2000**, *122*, 5644–5645. (b) Burdette, S. C.; Walkup, G. K.; Spingler, B.; Tsien, R. Y.; Lippard, S. J. *J. Am. Chem. Soc.* **2001**, *123*, 7831–7841. (c) Burdette, S. C.; Frederickson, C. J.; Bu, W.; Lippard, S. J. *J. Am. Chem. Soc.* **2003**, *125*, 1778–1787. (d) Chang, C. J.; Nolan, E. M.; Jaworski, J.; Burdette, S. C.; Sheng, M.; Lippard, S. J. *Chem. Biol.* **2004**, *11*, 203–210. (e) Nolan, E. M.; Lippard, S. J. *Inorg. Chem.* **2004**, *43*, 8310–8317. (f) Nolan, E. M.; Jaworski, J.; Okamoto, K. -I.; Hayashi, Y.; Sheng, M.; Lippard, S. J. *J. Am. Chem. Soc.* **2005**, *127*, 16812–16823. (g) Nolan, E. M.; Jaworski, J.; Racine, M. E.; Sheng, M.; Lippard, S. J. *Inorg. Chem.* **2006**, *45*, 9748–9757. (h) Nolan, E. M.; Ryu, J. W.; Jaworski, J.; Feazell, R. P.; Sheng, M.; Lippard, S. J. *J. Am. Chem. Soc.* **2006**, *128*, 15517–15528.

(9) Gee, K. R.; Zhou, Z. -L.; Qian, W. -J.; Kennedy, R. *J. Am. Chem. Soc.* **2002**, *124*, 776–778.

(10) Tang, B.; Huang, H.; Xu, K. H.; Tong, L. L.; Yang, G. W.; Liu, X.; An, L. G. *Chem. Commun.* **2006**, 3609–3611.

Published on Web 07/10/2009

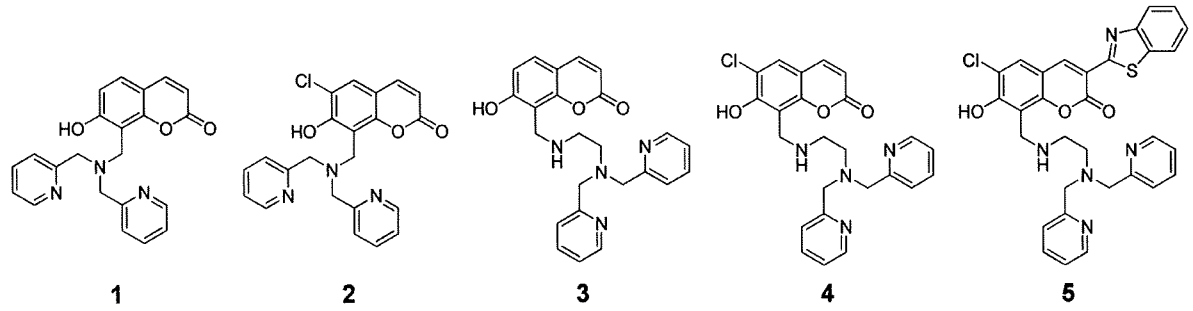

Figure 1. Structures of synthesized probes.

quinoline-based probes. Although such higher-intensity probes have several biological applications,[11] they suffer from a dependence on fluorescence intensity, in terms of dye localization or the intensity of the excitation light.

In the course of overcoming these drawbacks, ratiometric fluorescent probes for Zn^{2+} ions have been a recent focus.[12] Although there have been several ratiometric Zn^{2+} probes reported,[13] few can be practically used; in many cases, there are problems with short-wavelength excitation, low fluorescence intensity, low hydrophilicity, or elsewhere. Thus, we started developing ratiometric fluorescent Zn^{2+} probes for practical use in biological experiments.

We focused on coumarin as the fundamental platform of the fluorescent probes. Coumarins are known to be strongly fluorescent compounds, and it is easy to synthesize coumarin derivatives in general. For these reasons, coumarin-based probes are widely used in various biological assays.[14] In the case of fluorescence imaging, a coumarin-based fluorescent probe BTC is utilized for detecting Ca^{2+} in living cells.[15] Concerning Zn^{2+}-sensing probes, there have been several reports about coumarin-based fluorescent probes.[16] Brückner et al. reported of a ratiometric coumarin-based probe; however, the ratiometric property was achieved only in organic solvent.[16a,16b] In the case of other ratiometric probes, the metal selectivity and/or the cellular application was not demonstrated. Thus, there are currently no practical ratiometric Zn^{2+} probes based on a coumarin structure. Although recently Nagano et al. reported of a ratiometric probe based on an iminocoumarin structure,[13f] an iminocoumarin structure is potentially labile against hydrolysis. Therefore, there is still a great demand for ratiometric Zn^{2+} probes that can be used in imaging. We report here the design, synthesis, and photophysical properties of a series of ratiometric fluorescent Zn^{2+} probes based on a 7-hydroxycoumarin structure, after having investigated the cell membrane permeability and the ability to use Zn^{2+} in the ratiometric fluorescence imaging of living cells.

Results

Synthesis of Probes. First, we designed and synthesized a prototypical probe **1**, in only one step, from commercial compounds by using a Mannich-type reaction (Figure 1). We also designed and synthesized probes **2**–**5** by changing the ligand structure or substituting a coumarin structure (Figure 1). In the case of probe **2**, we introduced a chlorine atom at the 6-position for decreasing the pK_a of the 7-hydroxy group. In probe **3**, the ligand structure was modified; this substitution was expected to affect both the Zn^{2+}-binding affinity and the pK_a of the 7-hydroxy group. In probe **4**, we expected a cooperative effect from the introduced chlorine atom and the change in ligand structure. In probe **5**, a further substitution of a benzothiazolyl group was given at the 3-position of **4**. 3-Benzothiazolylcoumarin is the basic structure of a ratiometric Ca^{2+} probe BTC,[15] which can be excited with visible light; it is already in practical use. Thus, **5** was expected to be excited at the visible wavelength. Detailed synthesis schemes and procedures are described in the Supporting Information section.

Photophysical Properties of Probes. The excitation, emission, and absorption spectra of the prototypical probe **1** were measured (Figures 2(a), 3(a), and Supporting Information, Figure S1(a), respectively). The absorption spectra shifted toward longer wavelengths with the addition of Zn^{2+}, in a concentration-dependent manner. The peak top shifted from 331 to 357 nm. The maximum excitation wavelength also shifted with the addition of Zn^{2+}, and the fluorescence intensity largely increased. The emission spectra scarcely shifted ($\lambda_{max} \approx 450$ nm) because of the Zn^{2+} addition.

Meanwhile, the absorption and excitation spectra of the 6-chlorinated probe **2** showed a blue shift (λ_{ex}: 368 nm→ 362 nm, λ_{abs}: 367 nm → 360 nm) with the addition of Zn^{2+} (Figures 2(b) and Supporting Information, Figure S1(b)). The emission spectra also slightly shifted toward

(11) (a) Ueno, S.; Tsukamoto, M.; Hirano, T.; Kikuchi, K.; Yamada M. K.; Nishiyama, N.; Nagano, T.; Matsuki, N.; Ikegaya, Y. *J. Cell Biol.* **2002**, *158*, 215–220. (b) Qian, J.; Noebels, J. L. *J. Physiol.* **2005**, *566*, 747–758. (c) Yamasaki, S.; Sakata-Sogawa, K.; Hasegawa, A.; Suzuki, T.; Kabu, K.; Sato, E.; Kurosaki, T.; Yamashita, S.; Tokunaga, M.; Nishida, K.; Hirano, T. *J. Cell Biol.* **2007**, *177*, 637–645.

(12) See the following review: Carol, P.; Sreejith, S.; Ajayaghosh, A. *Chem. Asian J.* **2007**, *2*, 338–348.

(13) (a) Maruyama, S.; Kikuchi, K.; Hirano, T.; Urano, Y.; Nagano, T. *J. Am. Chem. Soc.* **2002**, *124*, 10650–10651. (b) Woodroofe, C. C.; Lippard, S. J. *J. Am. Chem. Soc.* **2003**, *125*, 11458–11459. (c) Chang, C. J.; Jaworski, J.; Nolan, E. M.; Sheng, M.; Lippard, S. J. *Proc. Natl. Acad. Sci. U.S.A.* **2004**, *101*, 1129–1134. (d) Taki, M.; Wolford, J. L.; O'Halloran, T. V. *J. Am. Chem. Soc.* **2004**, *126*, 712–713. (e) Kiyose, K.; Kojima, H.; Urano, Y.; Nagano, T. *J. Am. Chem. Soc.* **2006**, *128*, 6548–6549. (f) Komatsu, K.; Urano, Y.; Kojima, H.; Nagano, T. *J. Am. Chem. Soc.* **2007**, *129*, 13447–13454. (g) Zhang, Y.; Guo, X.; Si, W.; Jia, L.; Qian, X. *Org. Lett.* **2008**, *10*, 473–476. (h) Taki, M.; Watanabe, Y.; Yamamoto, Y. *Tetrahedron Lett.* **2009**, *50*, 1345–1347.

(14) (a) Goddard, J. P.; Raymond, J. L. *Trends Biotechnol.* **2004**, *22*, 363–370. (b) Katerinopoulos, H. E. *Curr. Pharm. Des.* **2004**, *10*, 3835–3852.

(15) Itaridou, H.; Foukaraki, E.; Kuhn, M. A.; Marcus, E. M.; Haugland, R. P.; Katerinopoulos, H. E. *Cell Calcium* **1994**, *15*, 190–198.

(16) (a) Lim, N. C.; Brückner, C. *Chem. Commun.* **2004**, 1094–1095. (b) Lim, N. C.; Schuster, J. V.; Porto, M. C.; Tanudra, M. A.; Yao, L.; Freake, H. C.; Brückner, C. *Inorg. Chem.* **2005**, *44*, 2018–2030. (c) Dakanali, M.; Roussakis, E.; Kay, A. R.; Katerinopoulos, H. E. *Tetrahedron Lett.* **2005**, *45*, 4193–4196. (d) Kulatilleke, C. P.; de Silva, S. A.; Eliav, Y. *Polyhedron* **2006**, *25*, 2593–2596. (e) Zhang, L.; Dong, S.; Zhu, L. *Chem. Commun.* **2007**, 1891–1893.

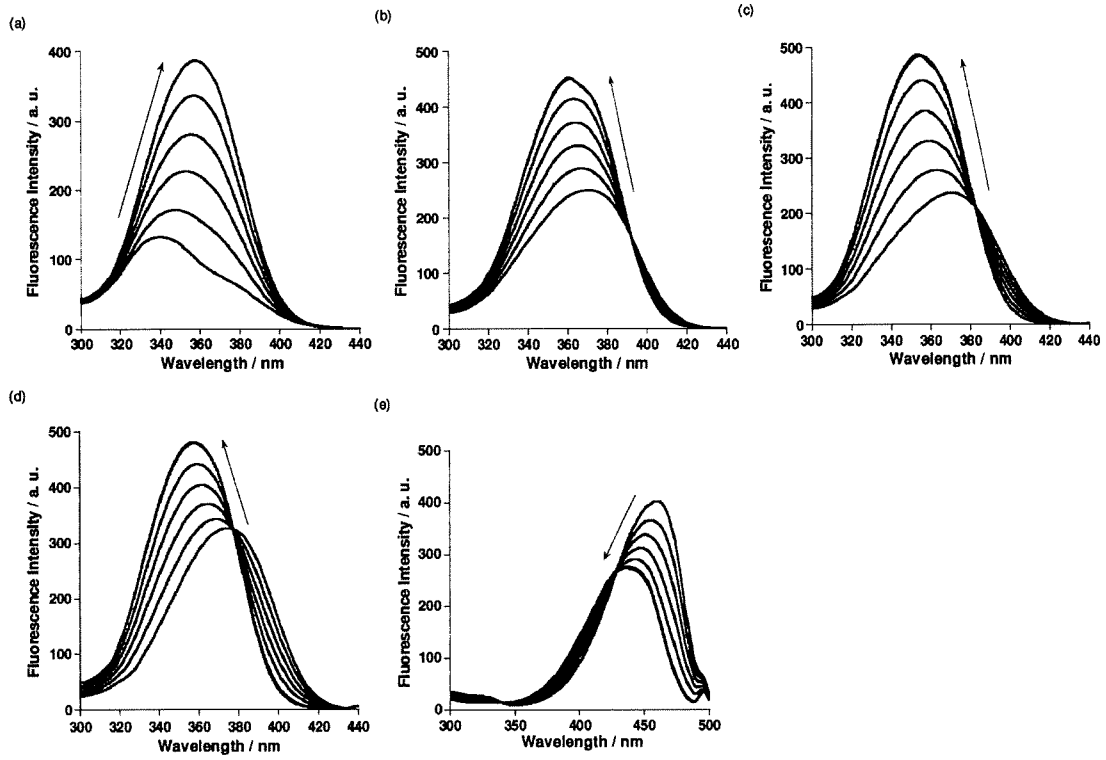

Figure 2. Excitation spectra of (a) 5 μM **1** (λ_{em} = 450 nm), (b) 5 μM **2** (λ_{em} = 445 nm), (c) 5 μM **3** (λ_{em} = 440 nm), (d) 5 μM **4** (λ_{em} = 443 nm), and (e) 1 μM **5** (λ_{em} = 494 nm), in the presence of various concentrations of Zn^{2+} (0, 0.2, 0.4, 0.6, 0.8, and 1.0 equiv to the probe concentration) in 100 mM HEPES buffer solution (pH 7.4). Arrows indicate the directions of the spectral changes as Zn^{2+} concentration increased.

shorter wavelengths, because of the Zn^{2+} addition (Figure 3(b)). The excitation, emission, and absorption spectra of **3**–**5** also showed blue shifts on account of adding Zn^{2+} (Figures 2(c)–(e), 3(c)–(e), and Supporting Information, Figure S1(c)–(e)).

We also investigated the fluorescence quantum yields of the synthesized compounds in the free form versus the Zn^{2+} complex form. The fluorescence quantum yields of probes **1**–**4** were increased by complexation with Zn^{2+}; all but **5** showed a remarkable change in fluorescence quantum yield. The photophysical data for the synthesized probes are summarized in Table 1.

Effect of pH on Photophysical Properties of Probes. We investigated the effect of solution pH on the photophysical properties of the synthesized probes. The absorption spectra of **1** at various solution pHs are shown in Figure 4(a). In acidic solution, the maximum absorption wavelength was at around 326 nm; in basic solution, however, the peak top shifted to 377 nm. In the case of probes **2**–**5**, their absorption spectra also showed red shifts as solution pH increased (Supporting Information, Figure S2).

Next, the effect of pH on the excitation spectrum of **1** was investigated. The fluorescence spectra of **1** at various solution pHs are shown in Figure 4(b). When the solution pH was increased from an acidic value, the fluorescence intensity increased; this trend continued until the pH was neutral, and the intensity then decreased when the pH was in excess of 8.

The fluorescence intensity of probes **1**–**5** at several solution pH points are plotted in Figure 4(c). Concerning all synthesized probes, the fluorescence intensity values decreased in the acidic and basic regions, although a control compound—7-hydroxy-8-methylcoumarin (HMC), which lacks a DPA ligand—did not show a fluorescence decrease at a basic-solution pH. Most probes, with the exception of **2**, showed virtually no physiological pH-sensitivity in the pH region of 7.4. The pK_a values of probes **1**–**5** were determined by pH titrating absorption measurements (Table 1). We also carried out potentiometric titration experiments (Supporting Information, Figure S5). For each compound, the pK_a value determined by absorbance titration was roughly consistent with one of the pK_a values determined by potentiometric titration (Supporting Information, Table S1).

Metal-Binding Properties. (1). Stoichiometry of Binding to Zn^{2+}. The binding stoichiometry of the probes to Zn^{2+} was investigated by Job's plot.[17] It was confirmed that all probes form 1:1 complexes with Zn^{2+} (Supporting Information, Figure S3).

(2). Apparent Binding Constants to Zn^{2+}. The apparent dissociation constants (K_d) of probes **1**–**5** in neutral aqueous buffer were determined by plotting the fluorescence intensity to free Zn^{2+} concentration (Supporting Information, Figure S4). The K_d values of probes **1**–**5** were in the range of 3.6–28 pM, as shown in Table 1.

(3). Metal-Sensing Selectivity. We investigated the fluorescence ratio values of the probes in response to various metal ions (Figure 5). The results of probes **1**–**4**

(17) Job, P. *Ann. Chim.* **1928**, *9*, 113–203.

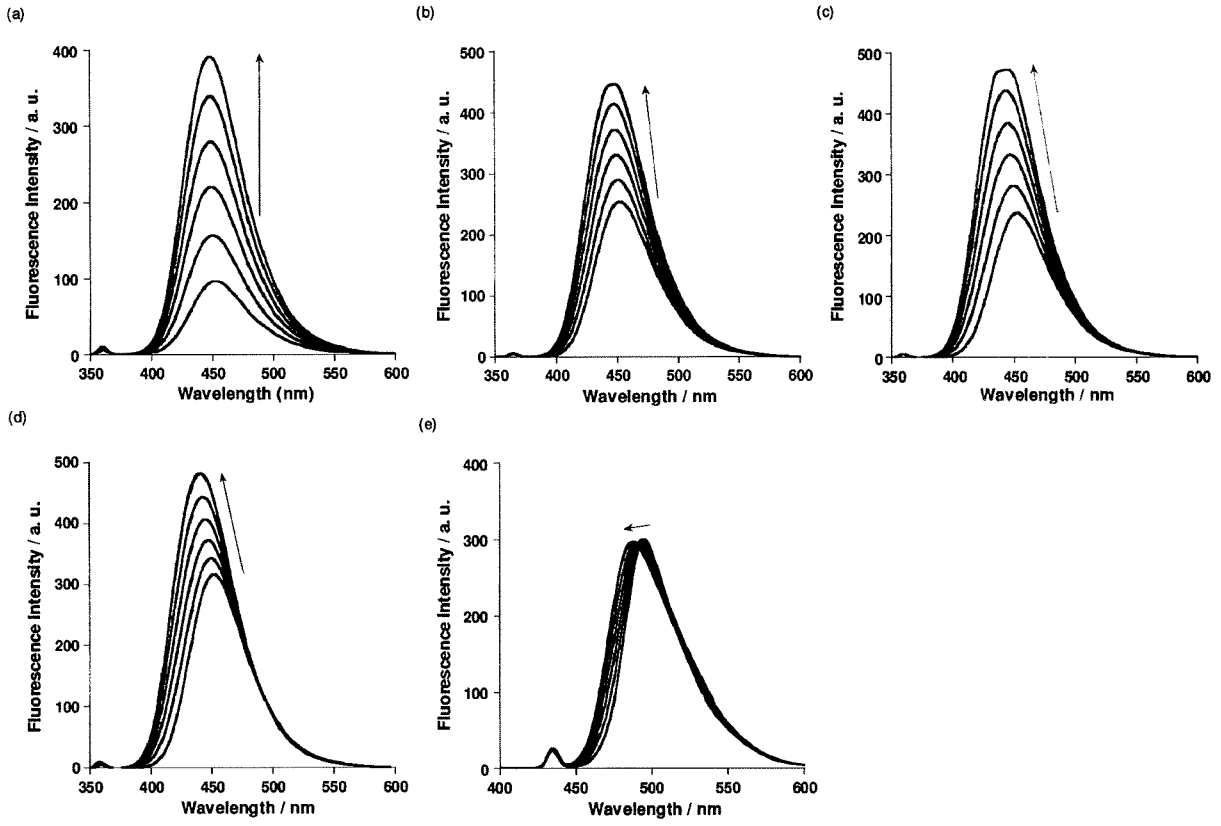

Figure 3. Emission spectra of (a) 5 μM **1** (λ_{ex} = 358 nm), (b) 5 μM **2** (λ_{ex} = 362 nm), (c) 5 μM **3** (λ_{ex} = 357 nm), (d) 5 μM **4** (λ_{ex} = 357 nm), and (e) 1 μM **5** (λ_{ex} = 432 nm), in the presence of various concentrations of Zn^{2+} (0, 0.2, 0.4, 0.6, 0.8, and 1.0 equiv to the probe concentration) in 100 mM HEPES buffer solution (pH 7.4). Arrows indicate the directions of the spectral changes as Zn^{2+} concentration increased.

Table 1. Physical Properties of Synthesized Probes

	absorption				excitation		emission		quantum yield			
	λ_{max}/nm ε/M^{-1} cm^{-1}				λ_{max}/nm		λ_{max}/nm		Φ		dissociation constant to Zn^{2+}	
compound	free		Zn^{2+}		free	Zn^{2+}	free	Zn^{2+}	free	Zn^{2+}	K_d/pM	pK_a[a]
1	331	12,300	357	16,500	344	358	451	450	0.41	0.66	28	8.9
2	367	15,100	360	17,600	368	362	450	445	0.51	0.71	14	4.0
3	369	14,100	351	18,000	374	357	452	443	0.46	0.83	5.2	6.3
4	372	19,700	354	19,100	374	357	450	440	0.52	0.80	5.0	3.7
5	442	51,500	423	48,500	454	432	494	487	> 0.96	> 0.99	3.6	2.5

[a] pK_a values determined by absorbance titration.

were quite similar to those of other probes that have a dipicolylamino group as the ligand. The fluorescence ratio values of all compounds were not affected by physiologically abundant metal ions such as Na^+, K^+, Mg^{2+}, or Ca^{2+}, even when the concentration of those metal ions were 5 mM—although Cd^{2+} also changed the fluorescence spectra. Regarding transition metals, Fe^{3+}, Co^{2+}, Ni^{2+}, and Cu^{2+} caused a quenching of the fluorescence.

Ratiometric Zn^{2+} Imaging in Living Cells. For the biological application, we first investigated cell permeability. RAW264 cells were incubated with our synthesized probes; of the five probes, only **5** successfully permeated the cells (Figure 6(a)). The ratiometric fluorescence images of the same picture as in Figure 6(a) were shown in Figure 6(b) top, where the cells were excited at two excitation wavelengths, 380 and 450 nm; the fluorescence ratio values were calculated with imaging software. Next, we investigated the Zn^{2+}-sensing ability of **5** in living cells. A total of 5 μM pyrithione as a Zn^{2+} ionophore and 50 μM Zn^{2+} were added to the cells, to increase the intracellular Zn^{2+} concentration $[Zn^{2+}]_i$. The ratio fluorescence values (F_{380}/F_{450}) were increased gradually, and became constant within several minutes; the pseudocolor changed purple or blue to yellow or green, which means the increase of the ratio fluorescence values (Figure 6(b) middle). Then, 100 μM TPEN (*N*,*N*,*N*′,*N*′-tetrakis(2-pyridylmethyl)ethylenediamine) was added, to decrease free $[Zn^{2+}]_i$ by chelating Zn^{2+}. The ratio fluorescence values were decreased to the background level with

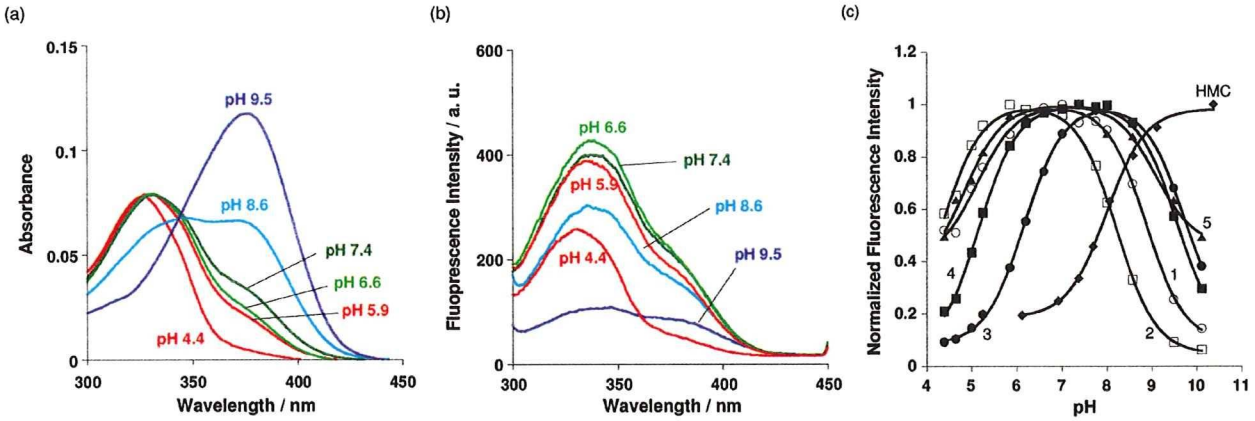

Figure 4. (a) Absorption and (b) excitation spectra (λ_{em} = 451 nm) of **1** at various solution pHs. (c) Effect of pH on fluorescence intensity of synthesized probes.

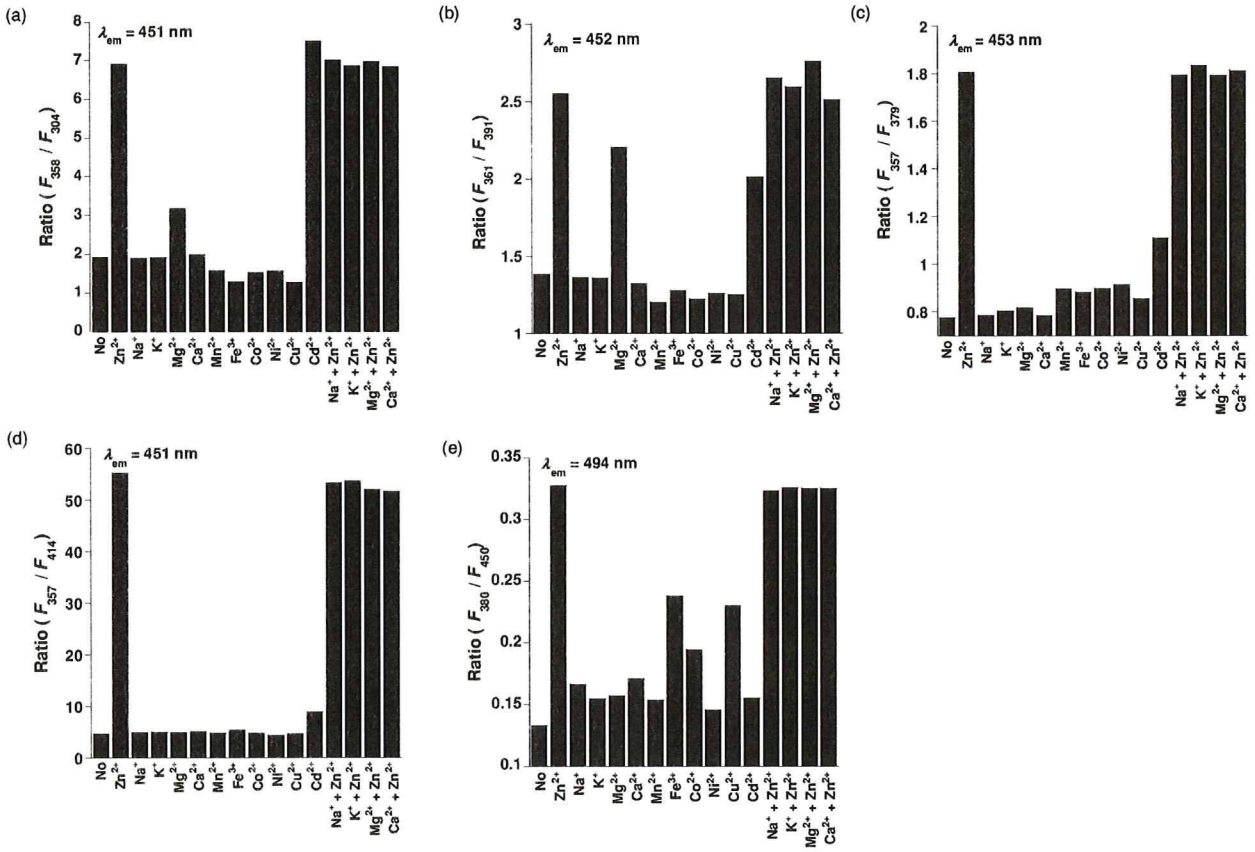

Figure 5. Metal-sensing selectivity of compounds (a) **1**, (b) **2**, (c) **3**, (d) **4**, and (e) **5**. F_x: fluorescence intensity excited at x nm. Na^+, K^+, Mg^{2+}, and Ca^{2+} were added at 1,000 times the concentration of the probes. Zn^{2+}, Mn^{2+}, Fe^{3+}, Ni^{2+}, Co^{2+}, Cu^{2+}, and Cd^{2+} were added at the equivalent concentration of the probes.

the pseudocolor getting back to the initial color (Figure 6(b) bottom). The time course of the fluorescence ratio values in three different areas indicated in Figure 6(a) were shown in Figure 6(c).

Discussion

Design of Prototypical Probe 1. First, we designed **1** as a prototypical compound of coumarin-based ratiometric Zn^{2+} probes (Figure 1). As the chromophore, we chose 7-hydroxycoumarin, also called umbelliferone, because of its strong fluorescence intensity and easy synthesis. As the metal ligand, a dipicolylamine (DPA) structure was chosen because of its high specificity, high stability, and fast complexation ability with Zn^{2+}. Although coumarin-based Zn^{2+} probes with a DPA ligand have been reported,[16b,16d] they did not exhibit ratiometric fluorescent

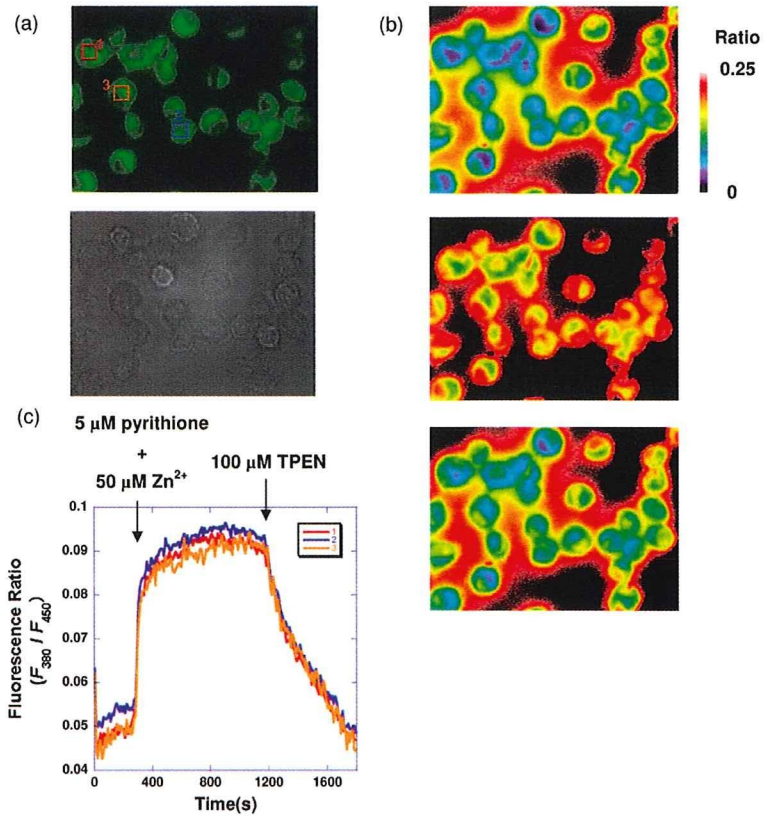

Figure 6. (a) Fluorescence microscopic image (λ_{ex}: 450 nm) (top), brightfield microscopic image (bottom), and (b) ratiometric fluorescence image (λ_{ex}: 380 and 450 nm) of RAW264 cells (top: 0 s, middle: 600 s, bottom: 1800 s) incubated with 10 μM **5** for 5 min at 37 °C. The color coding scale means the fluorescence ratio values. (c) Time course of the ratiometric fluorescence values of the areas 1 (red), 2 (blue), and 3 (orange), which are indicated in (a).

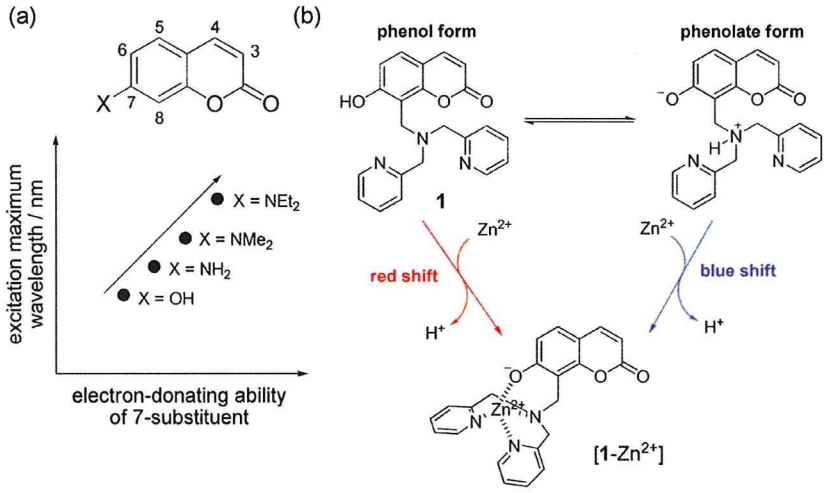

Figure 7. (a) Correlation between the electron-donating ability of 7-substituent and the excitation maximum wavelength of 7-substituted coumarins. (b) Two forms of probe **1** and the spectral change to the Zn^{2+} complex.

properties under physiological conditions. To achieve ratiometric Zn^{2+}-sensing, we focused our attention on the spectroscopic property of 7-substituted coumarins. As we had previously utilized the property for anion-sensing,[18] the absorbance and excitation spectra of the 7-substituted coumarin were affected by the functional substitution at the 7-position (Figure 7(a)).[19] When the oxygen atom of 7-hydroxy group coordinates Zn^{2+}, the absorption and the excitation spectra are expected to shift toward either

(18) Mizukami, S.; Nagano, T.; Urano, Y.; Odani, A.; Kikuchi, K. *J. Am. Chem. Soc.* **2002**, *124*, 3920–3924.

(19) Wheelock, C. E. *J. Am. Chem. Soc.* **1959**, *81*, 1348–1352.

longer or shorter wavelengths, according to changes in electron-donating ability. The direction of the excitation spectral shift would be dependent on whether the 7-hydroxy group is protonated or deprotonated under the measurement condition. Since the electron-donating ability is expected to be increased in the order of $-OH < -O^-\cdots Zn^{2+} < -O^-$, we expected spectral changes as follows: When the phenol form is dominant, the complexation with Zn^{2+} would prompt red shifts in the spectra; when the phenolate form is dominant, Zn^{2+} complexation would prompt blue shifts (Figure 7(b)).

Zn^{2+}-Sensing Properties of Probe 1. When Zn^{2+} was added to the solution of 5 μM **1**, the absorbance and the excitation spectra were shifted toward longer wavelengths (Supporting Information, Figure S1(a) and Figure 2(a), respectively). These results indicate that the 7-hydroxy group participated in the coordination with Zn^{2+}, and that the phenol form of **1** is dominant in 100 mM HEPES buffer (pH 7.4) (Figure 7(b)). This presumption was also confirmed by the pH profile measurement of the absorbance spectra (Figure 4(a)), where the peak top was around 330 nm at pH 7.4, as well as at a more acidic pH—although the peak top was around 370 nm at pH 9.5. The absorbance peak top of the 7-hydroxycoumarin was at 330 nm when the 7-hydroxy group was protonated, but shifted to 370 nm for the phenolate form.[20] According to the above mechanism, **1** made an excitation spectral shift toward a longer wavelength, with the addition of Zn^{2+} (Figure 2(a)); however, the spectral change was not ideal for ratiometric fluorescence imaging, because there was no clear isofluorescent point in the excitation spectra. On the other hand, an isosbestic point was observed in the absorbance spectra of **1** titrated with Zn^{2+} (Supporting Information, Figure S1(a)). This would be ascribed to the fluorescence quenching of **1**, because the fluorescence quantum yield (Φ) of **1** was lower than that of [**1**$-Zn^{2+}$] (Table 1). We considered the quenching to be the result of the photoinduced electron transfer (PET) from a DPA moiety, which would have been observed in known coumarin-based Zn^{2+} probes possessing a DPA ligand.[16b,16d]

Introduction of Chlorine Atom at the 6-Position of Coumarin: Design and Properties of Probe 2. In the case of **1**, the phenol form was expected to be dominant in pH 7.4, as described above. Conversely if the phenolate form is dominant, it will induce a blue shift of the excitation spectra. We considered that the difference in the way of spectral shift might enable the ratiometric measurement. Thus, we designed compound **2**, in which a chlorine atom was introduced at the 6-position. The substitution of a chloro- or fluoro-group at the 6-position can decrease the pK_a of 7-hydroxycoumarin via the inductive effect, and it was expected that the dominant form of **2** in pH 7.4 buffer was the deprotonated one.

The excitation spectral change of **2** (Figure 2(b)) showed that Zn^{2+} induced the blue shift of the excitation spectra. Also, the pH profile of the absorbance spectra of **2** indicated that the phenolate form of **2** was the dominant species at pH 7.4 because the absorbance maximum wavelength was 372 nm (Supporting Information, Figure S2(a)). Meanwhile, the difference in excitation maximum wavelength between **2** and [**2**$-Zn^{2+}$] was only 6 nm; therefore, further improvement was desired in terms of practical ratiometric fluorescence measurement, although there was an isofluorescent point in the excitation spectral change.

Modification of the Ligand Structure: Designs and Properties of Probes 3 and 4. We attempted to change the Zn^{2+} ligand structure because the modification of the ligand structure might not only change the association constant among metal ions but also change the pK_a of the hydroxy group near the ligand. We designed **3** and **4** with another ligand, *N*,*N*-dipicolylaminoethylamine. With regards to both **3** and **4**, the phenolate forms were dominant at pH 7.4 (Supporting Information, Figures S2(b) and S2(c)), and thus the addition of Zn^{2+} induced the blue shifts in the excitation spectra, as the case of **2** (Figures 2(c) and 2(d)).

The excitation maximum wavelengths of **3** and **4** were each 374 nm. When the probes bound Zn^{2+} ions, the spectral peak tops were shifted to 357 nm, and thus the spectral shifts were 17 nm each—much larger than had been the case with **1** or **2**. In the excitation spectra of **3** and **4**, in the presence of several concentrations of Zn^{2+} ion, there were isofluorescent points at 382 and 377 nm, respectively; therefore, they could serve as more practical ratiometric probes for Zn^{2+} ions. However, they are excitable only by UV light, which can cause damage to living cells and tissues. We therefore sought to improve further the probe structure for visible light excitation.

Design and Properties of Visible Light Excitation Probe 5. To achieve longer-wavelength excitation, further modification was required. Since deprotonated 3-benzothiazolyl-7-hydroxycoumarin is known to have strong absorption in the visible light region in polar solvent,[21] we designed and synthesized **5** based on this structure. As expected, the excitation maximum of **5** was at 454 nm for the deprotonated form as well as for **3** and **4**, and at 432 nm for the Zn^{2+} complex (Figure 2(e)). The isofluorescent point of the excitation spectra was observed at 428 nm. Thus, this probe can be used for ratiometric fluorescence measurement of Zn^{2+} with visible light excitation, for example, at 400 and 450 nm. In addition to the ratiometric fluorescence property derived by exciting at two different wavelengths, probe **5** could also be applied to ratiometric measurement by monitoring at two emission wavelengths. Figure 3(e) shows the emission spectral change in the presence of Zn^{2+}; the peak top shifted from 494 to 487 nm, with an isofluorescent point at 491 nm with Zn^{2+} addition. In passing, it should be noted that probe **4** also showed the same ratiometric emission properties.

Zn^{2+}-binding Properties of Probes 1–5. To study the Zn^{2+}-binding properties of the probes, the binding stoichiometry to Zn^{2+} was investigated. Job's plots showed that all probes formed 1:1 complexes with Zn^{2+} (Supporting Information, Figure S3). The apparent dissociation constants with Zn^{2+} were as high as with the known Zn^{2+} probes. Concerning the correlation between ligand structure and the apparent binding constant to Zn^{2+}, the dipicolylaminoethylamino group showed a

(20) Fink, D. W.; Koehler, W. R. *Anal. Chem.* **1970**, *42*, 990–993.

(21) Azim, S. A.; Al-Hazmy, S. M.; Ebeid, E. M.; El-Daly, S. A. *Opt. Laser Technol.* **2005**, *37*, 245–249.

slightly higher binding constant than did the dipicolylamino group. The sensing selectivity to Zn^{2+} was sufficient for cellular application, although the ratiometric values of probes are largely changed by Cd^{2+} ions, because Cd^{2+} does not constitute an important metal ion in physiological studies. In the case of **5**, the ratio values change by a small amount in response to Fe^{3+}, Cu^{2+}, and Co^{2+}; however, it is thought that these transition metal ions are generally bound to proteins and scarcely exist as free ions.

Cellular Application. To confirm whether **5** can detect intracellular Zn^{2+} under ratiometric fluorescence microscopy, we introduced the probe to RAW264 cells. Probe **5** could pass through the cell membrane without any modifications, as shown in Figure 6(a), probably because of the high lipophilicity involved. We then measured the change in ratiometric signal F_{380}/F_{450} by changing the intracellular Zn^{2+} concentration with pyrithione and TPEN. The results (Figure 6(b) and 6(c)) indicate that the probe enables the ratiometric detection of intracellular Zn^{2+} as quickly as the reported probes.[7c,8b] Since there are few compounds that can achieve both visual light excitation and ratiometric imaging in cells, we expect this probe can be utilized for the ratiometric detection of Zn^{2+} concentration in living cells that are vulnerable to UV excitation.

Conclusion

We developed a series of coumarin-based fluorescent probes for detecting Zn^{2+} with high affinities. The design strategy was based on the fluorescent properties of 7-substituted coumarins. The ligands were introduced at the 8-position because of the ease of synthesis and the electrostatic effects in reducing the pK_a of 7-hydroxy groups. Additional substituents were incorporated into the 6- and/or 3-position to improve the properties. Among five developed probes, **2**–**5** showed the ratiometric fluorescent properties, and **5** could be excited at visible light wavelength. Using cell membrane permeable probe **5**, we confirmed the ratiometric fluorescence-sensing ability for free Zn^{2+} in living cells. We expect this probe will lead to the "next stage" of physiological Zn^{2+} studies, in both neurology and immunology, and so on.

Experimental Section

Materials and Instruments. The detailed synthesis procedures for **1**–**5** are described in Supporting Information. All reagents for synthesis and measurements were purchased from Tokyo Chemical Industries, Wako Pure Chemical, or Aldrich Chemical Co. All were of the highest grade available, and were used without further purification. Silica gel column chromatography was performed using BW-300, or Chromatorex NH (Fuji Silysia Chemical Ltd.). Cells were obtained from the Riken BRC Cell Bank, and reagents for culture were purchased from Gibco. NMR spectra were recorded on a JEOL JNM-EX270 instrument at 270 MHz for ^1H NMR and at 64.5 MHz for ^{13}C NMR, or a JEOL JNM-AL400 instrument at 400 MHz for ^1H and at 100.4 MHz for ^{13}C NMR, using tetramethylsilane as an internal standard. Mass spectra (CI, FAB) were measured on a JEOL JMS-700. ESI-TOF MS was taken on a Waters LCT-Premier XE. UV–visible spectra were measured using a Shimadzu UV-1650PC. Fluorescence spectra were measured using a Hitachi F4500 spectrometer. The slit width for both excitation and emission spectra was 5.0 nm. The photomultiplier voltage was 400 V. For ratiometric fluorescence images were recorded using IX71 (Olympus) for the fluorescent microscope, Cool Snap HQ (Roper Scientific) for the cooled CCD camera, Polychrome V (TILL Photonics) for the xenon lamp with a monochromator, 470DCXRU (CHROMA) for the dichroic mirror, HQ515/50m-2p (CHROMA) for the emission filters, and MetaMorph (Universal Imaging Corporation) for the imaging software and data analysis.

Measurement of Photophysical Properties. All probes were prepared at 5 mM stock DMSO solution and diluted to the final concentration for each experiment. Zn^{2+} stock solution was prepared at 50 mM concentration by dissolving $ZnSO_4 \cdot 7H_2O$ in ultrapure water. Absorbance, excitation, and emission spectra were measured in 100 mM HEPES buffer (pH 7.4) at 25 °C. Quantum yields were calculated using quinine sulfate ($\Phi = 0.55$) in 0.5 M H_2SO_4 aq. or fluorescein ($\Phi = 0.92$) in 0.1 M NaOH aq. as the standard compounds, as described previously.[22]

Preparation of Zn^{2+}- and pH-Buffered Solution. A series of 100 mM HEPES buffer (pH 7.4, $I = 0.1$ ($NaNO_3$)) were prepared containing 10 mM nitrilotriacetic acid (NTA) and 0–5.3 mM $ZnSO_4$. The apparent stability constant for NTA-Zn^{2+} complex β_1' is defined as follows: $\beta_1' = \beta_1/\alpha_M\alpha_L$, where β_1 is the stability constant for NTA-Zn^{2+} complex, $\alpha_M = 1 + 10^{(pH - pK1)}$, $\alpha_L = 1 + 10^{(pKa1 - pH)} + 10^{(pKa1 + pKa2 - 2pH)} + 10^{(pKa1 + pKa2 + pKa3 - 3pH)}$. Regarding the pK_a of Zn^{2+}, $pK_1 = 9.0$,[23] and regarding the pK_as of NTA, $pK_{a1} = 9.74$, $pK_{a2} = 2.48$, and $pK_{a3} = 1.88$.[23] Protonation constants were corrected upward by 0.11 for 0.1 M of ionic strength.[24] The stability constant for NTA-Zn^{2+} complex: $\log\beta_1 = 10.4$.[23] Thus, $\alpha_M \approx 1$, $\alpha_L \approx 10^{2.34}$. $\beta_1' = \beta_1/\alpha_M\alpha_L = 10^{10.4}/10^{2.34} = 10^{8.06}$. Free Zn^{2+} concentration $[Zn^{2+}]_{free}$ was calculated as per the following equation.

$$[Zn^{2+}]_{free} = [Zn^{2+}]_{total}/(\beta_1'\alpha_M[NTA]_{free})$$
$$= [Zn^{2+}]_{total}/\{\beta_1'\alpha_M([NTA]_{total} - [Zn^{2+}]_{total})\}$$

Determination of the Apparent Dissociation Constant (K_d) with Zn^{2+}. The fluorescence intensity F of the probes were plotted against $[Zn^{2+}]_{free}$, the concentration of free Zn^{2+}. The apparent dissociation constants K_ds with Zn^{2+} were determined by fitting the data to the following equation:

$$F = F_0 + (F_{max} - F_0)[Zn^{2+}]_{free}/(K_d + [Zn^{2+}]_{free})$$

where F is the observed fluorescence intensity, F_0 is the fluorescence intensity without Zn^{2+}, F_{max} is the maximum fluorescence intensity, and $[Zn^{2+}]_{free}$ is the concentration of free Zn^{2+}.

Effect of pH on Fluorescence Properties. We measured the fluorescence intensity of the probes in 10 mM phosphate buffer aqueous solution showing several pH values (pH 4.4–12.5). The fluorescence intensities were plotted against solution pH.

Metal Ion Selectivity. The fluorescence intensity and ratio values were measured in 100 mM HEPES buffer (pH 7.4). The probe concentration was 5 μM for **1**–**4** or 1 μM for **5**. The stock solutions of Na^+, K^+, Ca^{2+}, and Mg^{2+} were prepared at 500 mM and diluted to final concentrations (5 mM or 1 mM). The stock solution of Mn^{2+}, Fe^{3+}, Co^{2+}, Ni^{2+}, Cu^{2+}, Zn^{2+}, and Cd^{2+} were prepared at 5 mM and diluted to final concentrations (5 μM or 1 μM).

Cell Cultures and Live Cell Imaging. RAW264 cells were cultured in MEM containing 10% fetal bovine serum, 1% penicillin, 1% streptomycin, and 0.1 mM MEM non-essential amino acid solution at 37 °C in a 5% CO_2 incubator. The cells

(22) Dawson, R. W.; Windsor, W. M. *J. Phys. Chem.* **1968**, *72*, 3251–3260.
(23) Perin, D. D.; Dempsey, B. *Buffers for pH and Metal Ion Control*; John Wiley & Sons, Chapman and Hall: New York and London, 1974.
(24) Martell, A. E.; Smith, R. M. *NIST Critical Stability Constants of Metal Complexes, NIST Standard Reference Database*; Plenum Press: New York and London, 1974; Vol. *1*.

were transferred to a glass-bottomed dish and incubated for 1 day before dye-loading. The cells were washed with PBS twice and incubated with PBS containing 10 μM probes for 5 min at 37 °C. The cells were then washed with PBS twice, and measurements were carried out with fluorescence microscope. A total of 5 μM pyrithione and 50 μM Zn^{2+} were treated to increase intracellular Zn^{2+} concentration, $[Zn^{2+}]_i$, and 100 μM TPEN was treated to decrease $[Zn^{2+}]_i$ by chelating.

Acknowledgment. This work was supported in part by the Ministry of Education, Culture, Sports, Science and Technology (MEXT) of Japan (Grants 18310144, 18032045, 18033034, 18011005, 19036012, 19021028, 19651093 to K.K. and 19710185 to S.M.). This work was also supported by the Special Coordination Funds for the Council of Science and Technology Policy Coordination Program of Science and Technology Projects, MEXT and JST, to K.K. K.K. was also supported by the Mitsubishi Foundation, by the Novartis Foundation for the Promotion of Science, by Shimadzu Science Foundation, by Kato Memorial Bioscience Foundation, by Astellas Foundation for Research on Metabolic Disorders, by the Uehara Memorial Foundation, by Terumo Life Science Foundation, by Nagase Science and Technology Foundation, and by the Asahi Glass Foundation. S.M. was supported by the Cosmetology Research Foundation.

Supporting Information Available: Detailed synthetic procedures of compounds, and supplementary figures. This material is available free of charge via the Internet at http://pubs.acs.org.

J|A|C|S COMMUNICATIONS

Published on Web 10/30/2009

Photoactive Yellow Protein-Based Protein Labeling System with Turn-On Fluorescence Intensity

Yuichiro Hori, Hideki Ueno, Shin Mizukami, and Kazuya Kikuchi*

Division of Advanced Science and Biotechnology, Graduate School of Engineering, Osaka University, 2-1 Yamadaoka, Suita, Osaka 565-0871, Japan

Received June 12, 2009; E-mail: kkikuchi@mls.eng.osaka-u.ac.jp

There has been considerable interest in bioimaging technologies for the clarification of protein functions in living systems. So far, fluorescent proteins have made a significant contribution to research on protein expression, localization, and protein−protein interaction.[1] Although various fluorescent proteins (FP) are currently known,[2] it is difficult to visualize proteins in deep tissues, because proteins emitting near-infrared fluorescence, which can pass through thick tissues, are lacking. In addition, the FP size is large (~27 kDa), and therefore, there has been a strong demand for the generation of a smaller protein tag.[3] As an alternative technology, protein labeling systems such as Halo-tag and CLIP-tag have been developed.[4] In these methods, a specific pair of a protein tag and its ligand is employed for detecting proteins of interest. The advantages of these methods are that a variety of fluorescent dyes are potentially available as labeling reagents including near-infrared probes and that the tag proteins are labeled in controlled time. However, in these systems, free probes must be removed by washing cells or purifying cell lysate to distinguish the fluorescence of bound and unbound probes. To solve this issue, our group recently reported on a fluorogenic labeling method.[5] But these tag proteins are still large.[4,5] Although there are some other techniques for protein labeling,[6] they have drawbacks in bioorthogonality or require additional enzyme for protein modification. To overcome these limitations, we utilized photoactive yellow protein (PYP) as a tag protein and developed labeling reagents for this protein, including a fluorogenic probe, which would not require any procedure for removing the free fluorescent probe.

PYP is a small, water-soluble protein found in several purple bacteria.[7] It consists of 125 amino acids (14 kDa) and binds to a natural cofactor, CoA thioester of 4-hydroxycinnamic acid, through transthioesterification with Cys69.[8] In addition to the natural cofactor, it is known that PYP binds to the thioester derivative of 7-hydroxycoumarin-3-carboxylic acid,[9] which is a fluorescent compound. Importantly, PYP and its ligands do not exist in animal cells and, thus, it is expected that PYP expressed in those cells could be bioorthogonally labeled by its exogenous ligand without any cross reaction by endogenous factors. With regard to the design of a fluorogenic labeling system, 7-hydroxycoumarin has an interesting fluorescent property as follows. Previous work shows that a coumarin derivative linked with fluorescein through a flexible linker has no or little fluorescence properties because of the intramolecular association between the dyes and their dissociation triggers the increase in fluorescence intensity.[10] Based on this principle, we designed a probe that consists of 7-hydroxycoumarin-3-carboxylic acid thioester connected to fluorescein through an ethylene glycol linker (Figure 1). It is considered that the probe in the absence of PYP is not fluorescent due to the intramolecular interaction and, once the probe binds to PYP, the coumarin is dissociated from the fluorescein because the interaction between the coumarin and PYP prevents the close contact of two fluorophores.

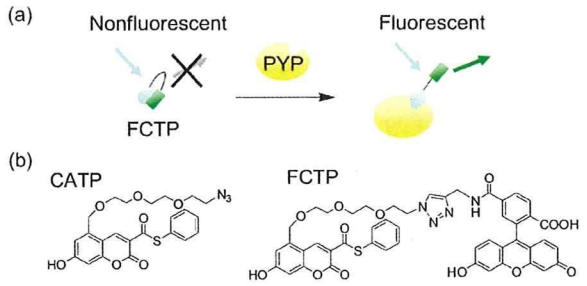

Figure 1. (a) Principle of fluorogenic labeling system based on PYP. (b) Structures of fluorescent probes, CATP and FCTP, for labeling PYP.

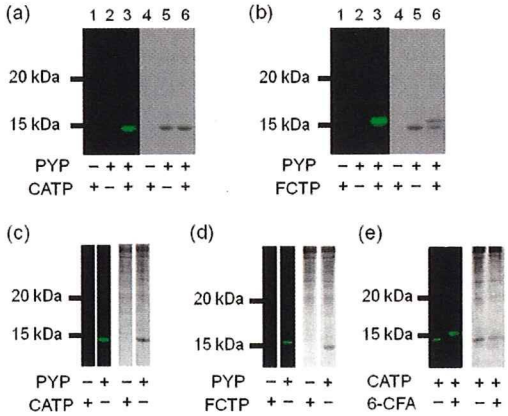

Figure 2. SDS-PAGE analyses of labeling reactions of PYP with probes, CATP and FCTP. Fluorescence and CBB-stained gel images are displayed on the left and right, respectively. PYP (10 μM) was reacted with CATP (25 μM) (a and c) or with FCTP (25 μM) (b and d). Images (c) and (d) represent the reactions in cell lysate. Image (e) represents the stepwise labeling of PYP (5 μM) with CATP (12.5 μM) and 6-CFA (200 μM) in cell lysate.

First, we synthesized CATP, which contains an azido group at the end of the linker (Figure 1b). Considering the steric hindrance, which is predicted from the structure of PYP with its natural cofactor,[11] the linker was introduced into the 5-position in the coumarin, because this position is assumed to be the 2-positon of the natural cofactor based on the structural similarity between these compounds. Then, fluorescein with an alkyne group (6-carboxy-fluorescein propalgylamide, 6-CFA) was conjugated to CATP by click chemistry to generate FCTP (Figure 1b). The probes were incubated with recombinant PYP purified from *E. coli*, and SDS-PAGE analysis was conducted to verify the binding of the probes to the protein (Figure 2a and b). In the absence of the probes, no fluorescence was detected in the gel. In the mixtures of the probes and PYP, fluorescent bands appeared, indicating that the probes bind to PYP. Interestingly, the reaction of FCTP and PYP yielded

10.1021/ja904800k CCC: $40.75

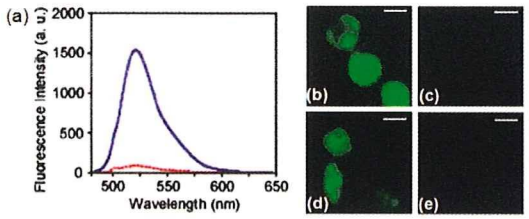

Figure 3. (a) Fluorescence spectra of FCTP (8 μM) in the absence (red dashed line) or presence (blue line) of PYP (5 μM). (b–e) Fluorescent live-cell imaging. Images (b, d) or (c, e) represent the cells that expressed or did not express PYP-PDGFRtm, respectively. The cells after incubation with CATP (5 μM; b, c) or FCTP (20 μM; d, e) are shown. Scale bars = 10 μm.

a slowly migrating band, which is regarded as FCTP-bound PYP because of its fluorescence. The binding of PYP and the probes was also confirmed by MALDI-TOF MS (Figure S1). The addition of CATP or FCTP to PYP gave the mass value of PYP bound to the individual probe, in which thiophenyl ester is replaced by thioester of Cys in the protein. The results indicate that the probes covalently bind to PYP through transthioesterification.

The binding specificity of the probes toward PYP was investigated. Labeling reactions of purified PYP were carried out in the lysate prepared from HEK293T cells. Figure 2c and d show that a single fluorescent band was detected only in the reaction mixture of PYP and each probe, confirming that PYP is specifically labeled by CATP or FCTP under this experimental condition. The influence of free thiols on the labeling reaction was also examined. The presence of a physiological concentration of glutathione (up to 10 mM) did not affect the labeling reactions (Figure S2).[13] Furthermore, the azido moiety of CATP would allow additional labeling of PYP with the second probe by click chemistry and could expand the range of the applications of this system. After the reaction of PYP and CATP in the cell lysate, 6-CFA was added to the reaction mixture in the presence of Cu^{2+} and tris(2-carboxyethyl)phosphine. Electrophoresis revealed a slowly migrating band, as is the case with the FCTP-bound PYP (Figure 2e). There were no newly appearing bands, demonstrating that the stepwise labeling reaction is quite specific.

To examine the fluorogenic properties of FCTP, the fluorescent spectra of the probes were measured (Figure 3a). In the absence of PYP, the fluorescence intensity of FCTP is very weak, suggesting that the coumarin and fluorescein dyes in the probe associate with each other. On the other hand, the binding of PYP and the probe leads to a dramatic increase in the fluorescence intensity. This increase is approximately 20-fold after 24 h of incubation. The result indicates that the coumarin dissociates from the fluorescein due to the formation of the complex between PYP and the probe. We then characterized the binding kinetics of PYP with CATP and FCTP by size exclusion chromatography and fluorescence measurement, respectively (Figures S3 and S4; see Supporting Information for the detailed procedure). The CATP reaction was almost complete within 2 h, consistent with a previous report, demonstrating the binding kinetics of a natural ligand to PYP.[12] In contrast, the binding of FCTP to PYP was slow, requiring more than 24 h to complete the reaction. One probable reason for this difference is that the intramolecular interaction in FCTP could influence its binding kinetics.

Finally, cell labeling experiments were conducted. HEK293T cells expressing PYP-PDGFRtm (the fusion protein of PYP and a transmembrane domain of platelet-derived growth factor receptor) on the cell membrane were prepared. CATP or FCTP was incubated with the cells in culture media. Fluorescence microscopy showed that fluorescent labeling by both probes occurred in the cells expressing PYP-PDGFRtm (Figures 3b and S5). No fluorescence was observed in the cells that did not express PYP-PDGFRtm, demonstrating that PYP is specifically labeled on the cell membrane by both probes. During the experiments, we noticed that CATP was cell-permeable. Therefore, intracellular imaging with CATP was also performed. After the labeling reaction of CATP and the cells expressing maltose binding protein-fused PYP (MBP-PYP) in cytosol, fluorescence was observed only in the cells expressing MBP-PYP, and not in the nonexpressing cells (Figure S5). This result clearly shows that CATP allows specific labeling of PYP inside living cells.

In conclusion, we have developed a protein labeling system, based on a small tag protein, PYP, and its fluorescent probes. The live-cell imaging and specific labeling of PYP were achieved by using CATP and FCTP. CATP has dual functions as a fluorescent probe and a chemical handle for two-step labeling. More importantly, FCTP shows fluorogenic characteristics, allowing the identification of the probe bound to its tag protein. These properties offer a more sophisticated application of this system to protein imaging studies.

Acknowledgment. This work was supported by MEXT of Japan. We thank Prof. Klaas J. Hellingwerf for providing the plasmid encoding PYP and Dr. Aya Fukuda for giving the plasmid for mammalian expression.

Supporting Information Available: Experimental procedures and supplemental results. This material is available free of charge via the Internet at http://pubs.acs.org.

References

(1) (a) Zaccolo, M. *Circ. Res.* **2004**, *94*, 866–873. (b) VanEngelenburg, S. B.; Palmer, A. E. *Curr. Opin. Chem. Biol.* **2008**, *12*, 60–65.
(2) (a) Shaner, N. C.; Steinbach, P. A.; Tsien, R. Y. *Nat. Methods* **2005**, *2*, 905–909. (b) Pakhomov, A. V.; Martynov, V. I. *Chem. Biol.* **2008**, *15*, 755–764.
(3) (a) Zhou, Z.; Koglin, A.; Wang, Y.; McMahon, A. P.; Walsh, C. T. *J. Am. Chem. Soc.* **2008**, *130*, 9925–9930. (b) Chen, I.; Ting, A. Y. *Curr. Opin. Biotechnol.* **2005**, *16*, 35–40.
(4) (a) Los, G. V.; Wood, K. *Methods Mol. Biol.* **2007**, *356*, 195–208. (b) Gautier, A.; Juillerat, A.; Heinis, C.; Corrêa, I. R., Jr.; Kindermann, M.; Beaufils, F.; Johnsson, K. *Chem. Biol.* **2008**, *15*, 128–136.
(5) Mizukami, S.; Watanabe, S.; Hori, Y.; Kikuchi, K. *J. Am. Chem. Soc.* **2009**, *131*, 5016–5017.
(6) (a) O'Hare, H. M.; Johnsson, K.; Gautier, A. *Curr. Opin. Struct. Biol.* **2007**, *17*, 488–494. (b) Wu, P.; Shui, W.; Carlson, B. L.; Hu, N.; Rabuka, D.; Lee, J.; Bertozzi, C. R. *Proc. Natl. Acad. Sci. U.S.A.* **2009**, *106*, 3000–3005. (c) Fernández-Suárez, M.; Baruah, H.; Martínez-Hernández, L.; Xie, K. T.; Baskin, J. M.; Bertozzi, C. R.; Ting, A. Y. *Nat. Biotechnol.* **2007**, *25*, 1483–1487. (d) Nonaka, H.; Tsukiji, S.; Ojida, A.; Hamachi, I. *J. Am. Chem. Soc.* **2007**, *129*, 15777–15779. (e) Adams, S. R.; Campbell, R. E.; Gross, L. A.; Martin, B. R.; Walkup, G. K.; Yao, Y.; Llopis, J.; Tsien, R. Y. *J. Am. Chem. Soc.* **2002**, *124*, 6063–6076.
(7) Kamiuchi, M.; Hara, M. T.; Stalcup, P.; Xie, A.; Hoff, W. D. *Photochem. Photobiol.* **2008**, *84*, 956–969.
(8) Kyndt, J. A.; Meyer, T. E.; Cusanovich, M. A.; Van Beeumen, J. J. *FEBS Lett.* **2002**, *512*, 240–244.
(9) van der Horst, M. A.; Arents, J. C.; Kort, R.; Hellingwerf, K. J. *Photochem. Photobiol. Sci.* **2007**, *6*, 571–579.
(10) Takakusa, H.; Kikuchi, K.; Urano, Y.; Higuchi, T.; Nagano, T. *Anal. Chem.* **2001**, *73*, 939–942.
(11) Anderson, S.; Crosson, S.; Moffat, K. *Acta Crystallogr., Sect. D* **2004**, *60*, 1008–1016.
(12) Imamoto, Y.; Ito, T.; Kataoka, M.; Tokunaga, F. *FEBS Lett.* **1995**, *374*, 157–160.
(13) Wu, G.; Fang, Y. Z.; Yang, S.; Lupton, J. R.; Turner, N. D. *J. Nutr.* **2004**, *34*, 489–492.

JA904800K

CHEMBIOCHEM

DOI: 10.1002/cbic.201000007

Noncovalent-Interaction-Promoted Ligation for Protein Labeling

Yuichiro Hori, Yuka Egashira, Ryosuke Kamiura, and Kazuya Kikuchi*[a]

Chemical labeling of proteins with fluorescent probes, isotopes, or other functional compounds provides valuable information that cannot be obtained through conventional biochemistry or molecular biology methods.[1,2] In particular, expressed protein ligation (EPL) is a powerful labeling method for analyzing protein function and structure, and has been widely applied to C-terminal labeling of proteins of interest (POI).[3] In EPL, proteins with a C-terminal thioester are linked to peptides (or proteins) with an N-terminal Cys by transthioesterification, and an amide bond is subsequently formed. The critical component of this technology is intein,[4] which is essential for generating thioester at the protein's C terminus. The major advantage of this technique is that the ligation reaction is considerably chemoselective and, thus, a desirable semisynthetic protein is reliably obtained. However, the reaction is generally inefficient and, therefore, a high concentration (mM or sub-mM) of reactants is required for efficient ligation.[2,3,5,6] Consequently, when the solubility of the reactants in water is low, a solubilization reagent, such as guanidine hydrochloride or a surfactant, is used to solubilize the reactants.[2,6] This limitation significantly hinders the application of this method to proteins that do not retain their structure and function after removal of the solubilizing reagent. In addition, barring a few exceptions,[7] this technique has not been applied to protein labeling in mammalian cell lysate or living cells because the protein expression level is not high enough for the ligation reaction. To overcome these obstacles, we developed a novel protein labeling method based on noncovalent interaction and intein-mediated ligation. This method allows efficient and specific protein labeling in cell lysate by using a low concentration range of thioester protein and synthetic peptide probe.

In order to attain efficient protein labeling, affinity tags were introduced into the reactants. This ensured that the local concentrations of the reactants would increase. As a result, it is expected that the ligation reaction would occur at low concentration. The affinity tags, Acid-a1 and Base-a1,[8] which form an antiparallel coiled coil, were chosen because these peptides are small (30 amino acids) and the interaction mechanism is well-known.[8,9] In the present research, interaction of the coiled coil was combined with the intein-mediated ligation for protein labeling (Scheme 1). Maltose binding protein (MBP) was employed as a model POI and Acid-a1 was fused to its C terminus (MBP-Acid). The intein was further connected to the C terminus of MBP-Acid to generate a fusion protein MBP-Acid-In, which could form a thioester in the C terminus of MBP-Acid. As a labeling reagent, fluorescein-conjugated Base-a1 (F-Base), which contains Cys at its N terminus, was prepared with Fmoc solid phase method. Acid-a1 with C-terminal thioester (Acid-T) was also synthesized for interaction analysis and model ligation with F-Base.

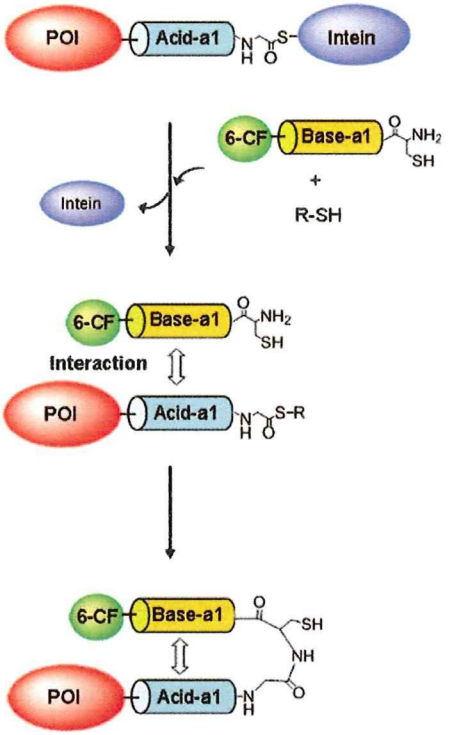

Scheme 1. Principle of protein labeling based on noncovalent coiled-coil interaction and intein-mediated ligation. Coiled coils are represented by Base-a1 and Acid-a1; POI: protein of interest; 6-CF: 6-carboxyfluorescein.

First, circular dichroism (CD) spectra were measured to determine whether coiled-coil interaction was retained despite the modification of the peptides and the fusion of Acid-a1 with protein domains. Both F-base and Acid-T showed a CD spectrum characteristic of disordered secondary structures (Figure 1 A). The addition of F-base to Acid-T resulted in a dramatic increase in negative Cotton effects at 208 and 222 nm. These results indicate that the peptides interact with each other to form α-helical structures. In contrast with the peptides, the CD spectrum of MBP-Acid-In in the absence of F-Base showed that MBP-Acid-In contains ordered secondary structures, including α-helices (Figure 1 B). This is consistent with previous reports on the crystal structures of those proteins.[10,11] The signal of MBP-Acid-In in the far-UV region intensified in the presence of F-Base; this demonstrates that the α-helix content increased. Thus, these results suggest that F-base

[a] Dr. Y. Hori, Y. Egashira, R. Kamiura, Prof. K. Kikuchi
Graduate School of Engineering, Osaka University
2-1 Yamadaoka, Suita, Osaka 565-0871 (Japan)
Fax: (+81) 6-6879-7875
E-mail: kkikuchi@mls.eng.osaka-u.ac.jp

Supporting information for this article is available on the WWW under http://dx.doi.org/10.1002/cbic.201000007.

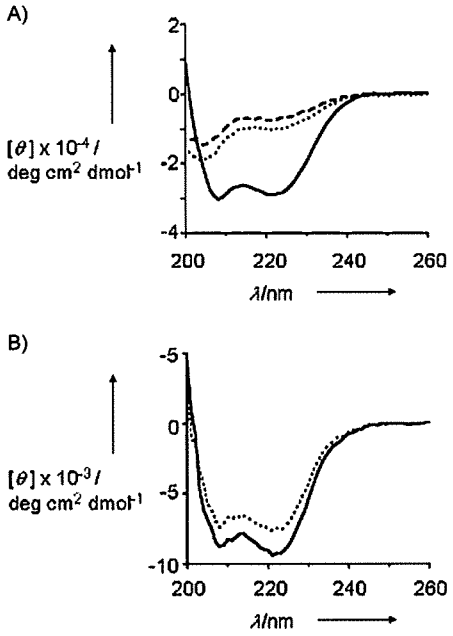

Figure 1. CD analyses of structural change in the coiled coils. A) CD spectra of F-Base (·----), Acid-T (•••••), and their complex (——). B) CD spectra of MBP-Acid-In in the absence (•••••) or presence (——) of F-Base.

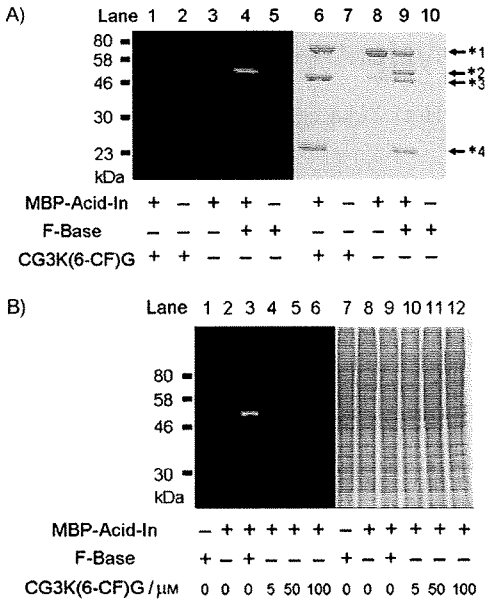

Figure 2. SDS-PAGE analyses of protein labeling experiments. Fluorescence and Coomassi Brilliant Blue-stained images are displayed on the left and right, respectively. MESNA (50 mM) was added to reaction mixtures only when they contained both MBP-Acid-In and peptide (F-Base or CG3K(6-CF)G). A) In vitro reactions of MBP-Acid-In (5 μM) with F-Base (5 μM) or CG3K(6-CF)G (5 μM) for 12 h at 25 °C. Asterisks 1–4 designate 69, 50, 46, and 23 kDa bands. B) Labeling reactions of MBP-Acid-In (5 μM) with F-Base (5 μM) or CG3K(6-CF)G (5, 50, or 100 μM) for 12 h at 25 °C in cell lysate.

binds to the segment of Acid-a1 in MBP-Acid-In and that this association induces the formation of the α-helix. Next, the model ligation reaction between F-Base and Acid-T was conducted by using low concentrations of peptides (10 μM). After a 12 h incubation period, the reaction mixture was analyzed by using HPLC (Figure S1 in the Supporting Information). Whereas the retention times of F-Base and Acid-T were 17 and 30 min, respectively, the sample after the reaction eluted at 20 min. ESI-TOF MS showed that the mass value of the eluted fraction was 8051.4, which corresponds to the theoretical mass value of the covalent ligation product (Figure S2 in the Supporting Information). This confirms that the reaction of the synthetic peptides can proceed in this concentration range.

Furthermore, the ligation reaction of F-Base and MBP-Acid-In was carried out in order to examine whether protein labeling occurs at a concentration of 5 μM. MBP-Acid-In was incubated with F-Base at 25 °C for 12 h and the labeling reaction was evaluated with SDS-PAGE. In addition to the band (69 kDa) representing MBP-Acid-In, three other bands appeared at 50, 46, and 23 kDa (Figure 2A). The band at 50 kDa corresponds to the molecular weight of F-base-conjugated MBP-Acid and was fluorescent, while the other two bands at 23 and 46 kDa can be assigned to intein and unligated MBP-Acid cleaved from MBP-Acid-In, respectively. These results indicate that MBP-Acid is labeled with F-base through a covalent bond and that the intein segment is removed as expected. This labeling reaction required MESNA (sodium 2-mercaptoethanesulfonate), which is also necessary in conventional EPL reactions.[2,3,5]

To verify the importance of the coiled-coil interaction, we carried out a labeling reaction with MBP-Acid-In and peptide CG3K(6-CF)G, which does not contain Base-a1, but has N-terminal Cys. Figure 2A shows that no fluorescent band derived from CG3K(6-CF)G was produced in lane 1 under these experimental conditions. This result clearly demonstrates that coiled-coil interaction is essential for efficient ligation. The strength of the noncovalent interaction between F-Base and MBP-Acid-In was investigated with fluorescent polarization assay in the absence of MESNA so that no ligation could occur (Figure 3). By conducting titration experiments, the dissociation constant was determined to be $(7.8 \pm 2.6) \times 10^{-8}$ M. The moderate affinity might not be sufficient for stable protein labeling with only the noncovalent interaction.[12] In contrast, in our method, the covalent ligation promoted by noncovalent interaction results in stable protein modification.

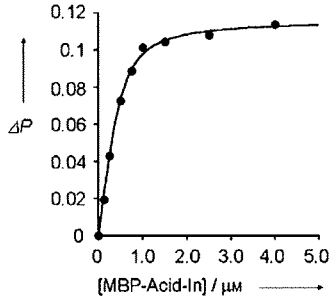

Figure 3. Determination of the dissociation constant of F-Base and MBP-Acid-In by a titration experiment. Change in fluorescence polarity (ΔP) of F-Base was plotted against the concentration of MBP-Acid-In.

Finally, in order to clarify the specificity of the labeling, a reaction in cell lysate was performed (Figure 2B). The lysate was prepared from HEK293T cells and added to the reaction mixture. A single fluorescent band was observed in the gel only when F-base was reacted with MBP-Acid-In, demonstrating that the labeling reaction is specific. Moreover, labeling with CG3K(6-CF)G was not detected despite the incubation of the peptide with MBP-Acid-In at a higher peptide concentration (100 μM). These results indicate that the presence of the coiled-coil interaction contributes significantly to specific protein labeling as well as to the reactivity of the probe.

In conclusion, we constructed a novel system for protein labeling by utilizing a coiled-coil tag and intein. The combination of a noncovalent interaction with a covalent ligation is an effective strategy for efficient and stable modification of proteins. Importantly, the size of the coiled-coil tag is small, and specific labeling is achieved in mammalian cell lysate by using a practical concentration of peptide-based labeling reagent and target protein. These properties are highly attractive for protein detection and visualization in a complex biological environment. Hence, this technique should provide a useful approach in biochemical and biological research.

Experimental Section

See the Supporting Information for experimental details.

Acknowledgements

This work was supported by MEXT of Japan (Grants 19021028, 19036012, 20011005, 20675004 to K.K. and 20790099 to Y.H.). We thank Prof. Shigenori Kanaya and Dr. Yuichi Koga at Osaka University for the use of CD spectropolarimeter, Prof. Kazuhiko Nakatani and Dr. Chikara Dohno at Osaka University for the use of MALDI-TOF mass spectrometer, and Prof. Shiroh Futaki and Dr. Ikuhiko Nakase at Kyoto University and Dr. Tatsuto Kiwada at Kanazawa University for giving advice on peptide synthesis.

Keywords: coiled coils · fluorescence · intein-mediated ligation · protein labeling · protein modifications

[1] a) I. Chen, A. Y. Ting, *Curr. Opin. Biotechnol.* **2005**, *16*, 35–40; b) J. A. Prescher, C. R. Bertozzi, *Nat. Chem. Biol.* **2005**, *1*, 13–21; c) S. S. Gallagher, J. E. Sable, M. P. Sheetz, V. W. Cornish, *ACS Chem. Biol.* **2009**, *4*, 547–556; d) A. Gautier, A. Juillerat, C. Heinis, I. R. Corrêa, Jr., M. Kindermann, F. Beaufils, K. Johnsson, *Chem. Biol.* **2008**, *15*, 128–136; e) M. K. So, H. Yao, J. Rao, *Biochem. Biophys. Res. Commun.* **2008**, *374*, 419–423.

[2] R. R. Flavell, P. Kothari, M. Bar-Dagan, M. Synan, S. Vallabhajosula, J. M. Friedman, T. W. Muir, G. Ceccarini, *J. Am. Chem. Soc.* **2008**, *130*, 9106–9112.

[3] a) K. Alexandrov, I. Heinemann, T. Durek, V. Sidorovitch, R. S. Goody, H. Waldmann, *J. Am. Chem. Soc.* **2002**, *124*, 5648–5649; b) J. P. Pellois, M. E. Hahn, T. W. Muir, *J. Am. Chem. Soc.* **2004**, *126*, 7170–7171; c) R. R. Flavell, T. W. Muir, *Acc. Chem. Res.* **2009**, *42*, 107–116; d) D. Schwarzer, P. A. Cole, *Curr. Opin. Chem. Biol.* **2005**, *9*, 561–569.

[4] T. C. Evans, Jr., M. Q. Xu, *Biopolymers* **1999**, *51*, 333–342.

[5] a) U. Arnold, M. P. Hinderaker, B. L. Nilsson, B. R. Huck, S. H. Gellman, R. T. Raines, *J. Am. Chem. Soc.* **2002**, *124*, 8522–8523; b) P. S. Hauser, R. O. Ryan, *Protein Expression Purif.* **2007**, *54*, 227–233.

[6] D. Schwarzer, Z. Zhang, W. Zheng, P. A. Cole, *J. Am. Chem. Soc.* **2006**, *128*, 4192–4193.

[7] a) R. Y. Lue, G. Y. Chen, Y. Hu, Q. Zhu, S. Q. Yao, *J. Am. Chem. Soc.* **2004**, *126*, 1055–1062; b) L. P. Tan, R. Y. Lue, G. Y. Chen, S. Q. Yao, *Bioorg. Med. Chem. Lett.* **2004**, *14*, 6067–6070.

[8] M. G. Oakley, P. S. Kim, *Biochemistry* **1998**, *37*, 12603–12610.

[9] E. K. O'Shea, K. J. Lumb, P. S. Kim, *Curr. Biol.* **1993**, *3*, 658–667.

[10] F. A. Quiocho, J. C. Spurlino, L. E. Rodseth, *Structure* **1997**, *5*, 997–1015.

[11] T. Klabunde, S. Sharma, A. Telenti, W. R. Jacobs, Jr., J. C. Sacchettini, *Nat. Struct. Biol.* **1998**, *5*, 31–36.

[12] a) L. W. Miller, Y. Cai, M. P. Sheetz, V. W. Cornish, *Nat. Methods.* **2005**, *2*, 255–257; b) H. E. Rajapakse, D. R. Reddy, S. Mohandessi, N. G. Butlin, L. W. Miller, *Angew. Chem.* **2009**, *121*, 5090–5092; *Angew. Chem. Int. Ed.* **2009**, *48*, 4990–4992.

Received: January 5, 2010
Published online on February 19, 2010

OPEN ACCESS Freely available online

PLoS one

Ablation of NMDA Receptors Enhances the Excitability of Hippocampal CA3 Neurons

Fumiaki Fukushima[1], Kazuhito Nakao[1], Toru Shinoe[2¤a], Masahiro Fukaya[3], Shin-ichi Muramatsu[4], Kenji Sakimura[5], Hirotaka Kataoka[1], Hisashi Mori[1¤b], Masahiko Watanabe[3], Toshiya Manabe[2,6], Masayoshi Mishina[1]*

1 Department of Molecular Neurobiology and Pharmacology, Graduate School of Medicine, University of Tokyo, Tokyo, Japan, **2** Division of Neuronal Network, Institute of Medical Science, University of Tokyo, Tokyo, Japan, **3** Department of Anatomy, Hokkaido University School of Medicine, Sapporo, Japan, **4** Division of Neurology, Department of Medicine, Jichi Medical University, Tochigi, Japan, **5** Department of Cellular Neurobiology, Brain Research Institute, Niigata University, Niigata, Japan, **6** CREST, JST, Kawaguchi, Japan

Abstract

Synchronized discharges in the hippocampal CA3 recurrent network are supposed to underlie network oscillations, memory formation and seizure generation. In the hippocampal CA3 network, NMDA receptors are abundant at the recurrent synapses but scarce at the mossy fiber synapses. We generated mutant mice in which NMDA receptors were abolished in hippocampal CA3 pyramidal neurons by postnatal day 14. The histological and cytological organizations of the hippocampal CA3 region were indistinguishable between control and mutant mice. We found that mutant mice lacking NMDA receptors selectively in CA3 pyramidal neurons became more susceptible to kainate-induced seizures. Consistently, mutant mice showed characteristic large EEG spikes associated with multiple unit activities (MUA), suggesting enhanced synchronous firing of CA3 neurons. The electrophysiological balance between fast excitatory and inhibitory synaptic transmission was comparable between control and mutant pyramidal neurons in the hippocampal CA3 region, while the NMDA receptor-slow AHP coupling was diminished in the mutant neurons. In the adult brain, inducible ablation of NMDA receptors in the hippocampal CA3 region by the viral expression vector for Cre recombinase also induced similar large EEG spikes. Furthermore, pharmacological blockade of CA3 NMDA receptors enhanced the susceptibility to kainate-induced seizures. These results raise an intriguing possibility that hippocampal CA3 NMDA receptors may suppress the excitability of the recurrent network as a whole *in vivo* by restricting synchronous firing of CA3 neurons.

Citation: Fukushima F, Nakao K, Shinoe T, Fukaya M, Muramatsu S-i, et al. (2009) Ablation of NMDA Receptors Enhances the Excitability of Hippocampal CA3 Neurons. PLoS ONE 4(1): e3993. doi:10.1371/journal.pone.0003993

Editor: Frederic Andre Meunier, The University of Queensland, Australia

Received September 4, 2008; **Accepted** December 3, 2008; **Published** January 14, 2009

Funding: This work was supported in part by Grant-in-Aid for Scientific Research on Priority Areas (Molecular Brain Science) and Global COE Program (Integrative Life Science Based on the Study of Biosignaling Mechanisms) from the Ministry of Education, Culture, Sports, Science and Technology of Japan. F.F. was supported by Japan Society for the Promotion of Science, and S.T. by the 21st Century COE Program, the Ministry of Education, Culture, Sports, Science and Technology of Japan. The funders had no role in study design, data collection and analysis, decision to publish, or preparation of the manuscript.

Competing Interests: The authors have declared that no competing interests exist.

* E-mail: mishina@m.u-tokyo.ac.jp

¤a Current address: Division of Molecular and Developmental Biology, Institute of Medical Science, University of Tokyo, Tokyo, Japan,
¤b Current address: Department of Molecular Neuroscience and Pharmaceutical Sciences, Graduate School of Medicine, University of Toyama, Toyama, Japan

Introduction

Hippocampal CA3 pyramidal neurons form abundant recurrent connections with other CA3 neurons [1,2]. The activity of single pyramidal neurons spreads to other CA3 neurons and this facilitates the rapid synchronization of action-potential firing in CA3 neurons [3]. Synchronized discharges of hippocampal CA3 neurons are supposed to underlie network oscillations [4], memory consolidation [5] and seizure generation [6]. Physiological sharp wave (SPW) activity that occurs during slow-wave sleep and behavioral immobility is dependent on synchronous discharges by population of CA3 pyramidal neurons [7,8]. Synchronized CA3 activity may also contribute to the pathological EEG pattern, known as an interictal spike, which indicates a propensity for temporal lobe seizures [6].

NMDA receptors play key roles in synaptic plasticity and memory [9]. In the CA3 network, NMDA receptors are abundant at the commissural/associational synapses but scarce at the mossy fiber synapses [10]. Thus, the CA3 recurrent network is under the control of NMDA receptors. NMDA receptors in the hippocampal CA3 region are implied in rapid acquisition and recall of associative memory as well as paired associate learning [11–13]. On the other hand, studies with hippocampal slices showed that the synchronous network activity induces NMDA receptor-dependent LTP of CA3 recurrent synapses [14] and that stimuli that induced NMDA receptor-dependent LTP in the CA3 region generated sharp wave-like synchronous network activity [15]. These *in vitro* observations raised the hypothesis that the NMDA receptor-mediated LTP contributes to the generation of synchronous network activity. Here, we generated hippocampal CA3 pyramidal neuron-specific NMDA receptor mutant mice on the pure C57BL/6N genetic background. The ablation of hippocampal CA3 NMDA receptors resulted in the enhancement of the susceptibility to kainate-induced seizure and the emergence of characteristic large EEG spikes. We also showed that the virus-mediated ablation of hippocampal CA3 NMDA receptors in the